Graz University of Technology

Master's Thesis

Refractory Wear Modelling using Statistical Methods

conducted at the
Signal Processing and Speech Communications Laboratory
Graz University of Technology, Austria

in co-operation with
RHI AG
Vienna, Austria

by
Markus Feuerstein

Supervisor:
Franz Pernkopf

Graz, September 8, 2016

Abstract

Steel is one of the world's most important resources and our standard of living wouldn't be possible without it. Cars, skyscrapers, planes, power lines, natural-gas pipelines - the list is endless. Neither of those things would be possible without steel. Therefore many companies conduct research to optimize the processes involved in steelmaking. This thesis is part of the APO project ("Automatische Pflegeoptimierung") from RHI AG. The RHI AG is one of the world's leading refractory material and maintenance robot manufacturer.
Maintenance in a steel plant is crucial for safely operating a steel plant and extending the lifetime of an electric arc furnace (EAF). The long term goal of APO is to extend the lifetime of such a furnace and therefore propose and automatically execute maintenance actions. One important step towards this goal is to predict the remaining useful lifetime (RUL) of a furnace according to a production plan. The prediction of the RUL, i.e., the prediction of the wear of the refractory is the subject of this thesis.
For the prediction of the refractory wear we design and evaluate three linear models that make use of the well-known Kalman filter. The first model heavily relies on the wear rates of the most frequent steel grades which are previously calculated from an overdetermined system of linear equations. The second model is designed for adaption of the wear rate during the lifetime of an EAF but also relies on a modified version of the control inputs. The third model is designed to adapt the wear of the most common steel grades and the maintenance actions separately.
All three models are evaluated individually. We show that all three models promise good prediction results as long as the ground truth data, i.e., the laser measurements are plausible. In a further step, we compare all three models. This comparison leads to the conclusion that the performance of the three models is similarly good with the exception of Model Two. At average, Model Two has a slightly higher error. We show that all three models are able to predict the wear of the refractory of an EAF.

Kurzfassung

Stahl is eine der wichtigsten Ressourcen der Welt und unser Lebensstandard wäre ohne Stahl nicht möglich. Autos, Hochhäuser, Flugzeuge, Stromleitungen, Gas Pipelines - die Liste ist endlos. All dies wäre ohne Stahl nicht möglich. Aus diesem Grund forschen viele Firmen an den Prozessen, die in die Produtkion von Stahl involviert sind. Diese Arbeit ist ein Teil von APO ("Automatische Pflegeoptimierung"), ein Projekt der RHI AG. Die RHI AG ist ein weltweit führender Hersteller von Feuerfest-Produkten und Pflege-Robotern.
Die Pflege und Wartung eines Elektrolichtbogenofens in einem Stahlwerk ist ein wichtiger Punkt um die Sicherheit zu gewährleisten und die Lebensdauer eines solchen Ofens zu erhöhen. Das Langzeitziel von APO ist es, die Verwendungsdauer eines Elektrolichbogenofens zu erhöhen. Dazu sollen optimale Pflegezeitpunkte vorgeschlagen und in weiterer Folge sollen die Pflegemaßnahmen automatisiert durchgeführt werden. Dafür muss zuerst eine Methode gefunden werden um die Lebenszeit eines Elektrolichbogenofens vorherzusagen. Diese Vorhersage ist das Thema dieser Arbeit.
Für diese Vorhersage wurden drei lineare Modelle entwickelt, die sich den Kalman Filter zu Nutze machen. Das erste Modell besteht aus einem eindimensionalen Kalman Filter mit "Control Inputs". Diese "Control Inputs" wurden vorab aus einem überdefinierten linearen Gleichungssystem bestimmt. Das zweite Modell basiert ebenfalls auf diesen "Control Inputs", ist jedoch ein zweidimensionaler Kalman Filter und bietet somit eine gewisse Anpassungsfähigkeit an die vergangenen Verschleißraten. Das dritte Modell versucht den Verschleiß der am häufigsten auftretenden Stahlsorten und den Einfluss der Pflege zu modellieren um sich flexibler anpassen zu können.
Alle drei Modelle werden zuerst einzeln evaluiert. Es wird gezeigt, dass alle drei Modelle eine gute Vorhersage liefern solange die zugrunde liegenden Laserdaten korrekt sind. In einem weiteren Schritt werden alle drei Modelle miteinander verglichen. Dieser Vergleich führt zu der Schlussfolgerung, dass alle drei Modelle ungefähr gleich gute Vorhersagen liefern. Eine Ausnahme bildet Modell Zwei welches im Durchschnitt einen leicht höheren Vorhersagefehler hat als die anderen zwei Modelle. Es wird gezeigt, dass es mit Hilfe dieser linearen Modelle möglich ist die Lebensdauer eines Elektrolichtbogenofens vorherzusagen.

Acknowledgements

First and foremost, I would like to thank my parents for their love and support throughout my life and my studies.
This thesis was conducted at the Signal Processing and Speech Communications Laboratory at the University of Technology in Graz, Austria, in cooperation with RHI AG in Vienna, Austria. I like to thank the RHI AG, particularly Gregor Lammer for giving me the opportunity of this research.
I also would like to thank Franz Pernkopf for his invaluable guidance and support throughout this thesis.
Last but not least, I want to thank all my friends and colleagues who have accompanied me during the course of my studies.

Statutory Declaration

I declare that I have authored this thesis independently, that I have not used other than the declared sources/resources, and that I have explicitly marked all material which has been quoted either literally or by content from the used sources.

date	(signature)

Contents

1 Introduction **7**
1.1 Steelmaking - Two Different Furnaces . . . 7
1.2 Steelmaking with the Electric Arc Furnace . . . 9
1.2.1 Furnace Charging . . . 9
1.2.2 Melting . . . 9
1.2.3 Refining . . . 10
1.2.4 De-slagging . . . 10
1.2.5 Tapping . . . 10
1.2.6 Furnace Turn-around . . . 10
1.3 Motivation . . . 11
1.4 Involved Companies . . . 12
1.4.1 RHI AG . . . 12
1.4.2 Emirates Steel . . . 12
1.4.3 Process Metrix . . . 12

2 Theory and Background **13**
2.1 Least Squares Method . . . 13
2.2 Kalman Filter . . . 15
2.3 Data Set . . . 20
2.3.1 Laser Measurements . . . 20
2.3.2 Production Data . . . 21
2.3.3 Maintenance Data . . . 21
2.3.4 Hot Spots . . . 21

3 Approach and Implementation **23**
3.1 Least Squares Model . . . 24
3.1.1 Approach . . . 24
3.1.2 Implementation . . . 24
3.2 Kalman Filter - Model One . . . 26
3.2.1 Approach . . . 26
3.2.2 Implementation . . . 27
3.3 Kalman Filter - Model Two . . . 28
3.3.1 Approach . . . 28
3.3.2 Implementation . . . 29
3.4 Kalman Filter - Model Three . . . 30
3.4.1 Approach . . . 30
3.4.2 Implementation . . . 31

4 Evaluation **33**
4.1 Least Squares Evaluation . . . 33
4.2 Model One Evaluation . . . 35
4.3 Model Two Evaluation . . . 39
4.4 Model Three Evaluation . . . 42
4.5 Comparison . . . 45
4.6 Insights on Q and R . . . 47
4.7 Quality of Laser Measurments . . . 50

5 Conclusion and Future Work **53**
5.1 Conclusion . . . 53

5.2 Future Work 54

Abbreviations

AC Alternating Current

APO Automatische Pflegeprogrammoptimierung - Intelligent Maintenance Optimization

BOF Basic Oxygen Furnace

DC Direct Current

DRI Direct Reduced Iron

EAF Electric Arc Furnace

RMSE Root Mean Squared Error

RUL Remaining Useful Life

1 Introduction

Contents

1.1 Steelmaking - Two Different Furnaces 7
1.2 Steelmaking with the Electric Arc Furnace 9
1.2.1 Furnace Charging 9
1.2.2 Melting 9
1.2.3 Refining 10
1.2.4 De-slagging 10
1.2.5 Tapping 10
1.2.6 Furnace Turn-around 10
1.3 Motivation 11
1.4 Involved Companies 12
1.4.1 RHI AG 12
1.4.2 Emirates Steel 12
1.4.3 Process Metrix 12

This chapter introduces the process of steelmaking. Steel is one of the most important resources in the world and our standard of living wouldn't be possible without it. Cars, skyscrapers, planes, power lines, natural-gas pipelines, the list is endless, neither of those would be possible without steel. Therefore a lot of research has been conducted in the area of steelmaking and improving the involved processes. The demand of steel today is bigger than ever.

First, we shortly introduce the two basic approaches to produce steel and then introduce the steelmaking process with an electric arc furnace in more detail. After this overview of the steelmaking process, we introduce further steelmaking terminology used throughout this thesis. Furthermore, the critical and time consuming aspects of refractory wear maintenance are described and the involved companies are introduced.

1.1 Steelmaking - Two Different Furnaces

Basically there exist two different processes to make steel:

- Basic oxygen furnace (BOF)
- Electric arc furnace (EAF)

The BOF uses around 25-35 percent of old steel (scrap) while the rest is liquid hot metal which is delivered from a blast furnace to produce new steel. On the other hand the EAF uses almost 100 percent of scrap or direct reduced iron (DRI) to produce new steel [1]. In this thesis the main focus lies on the electric arc furnace.

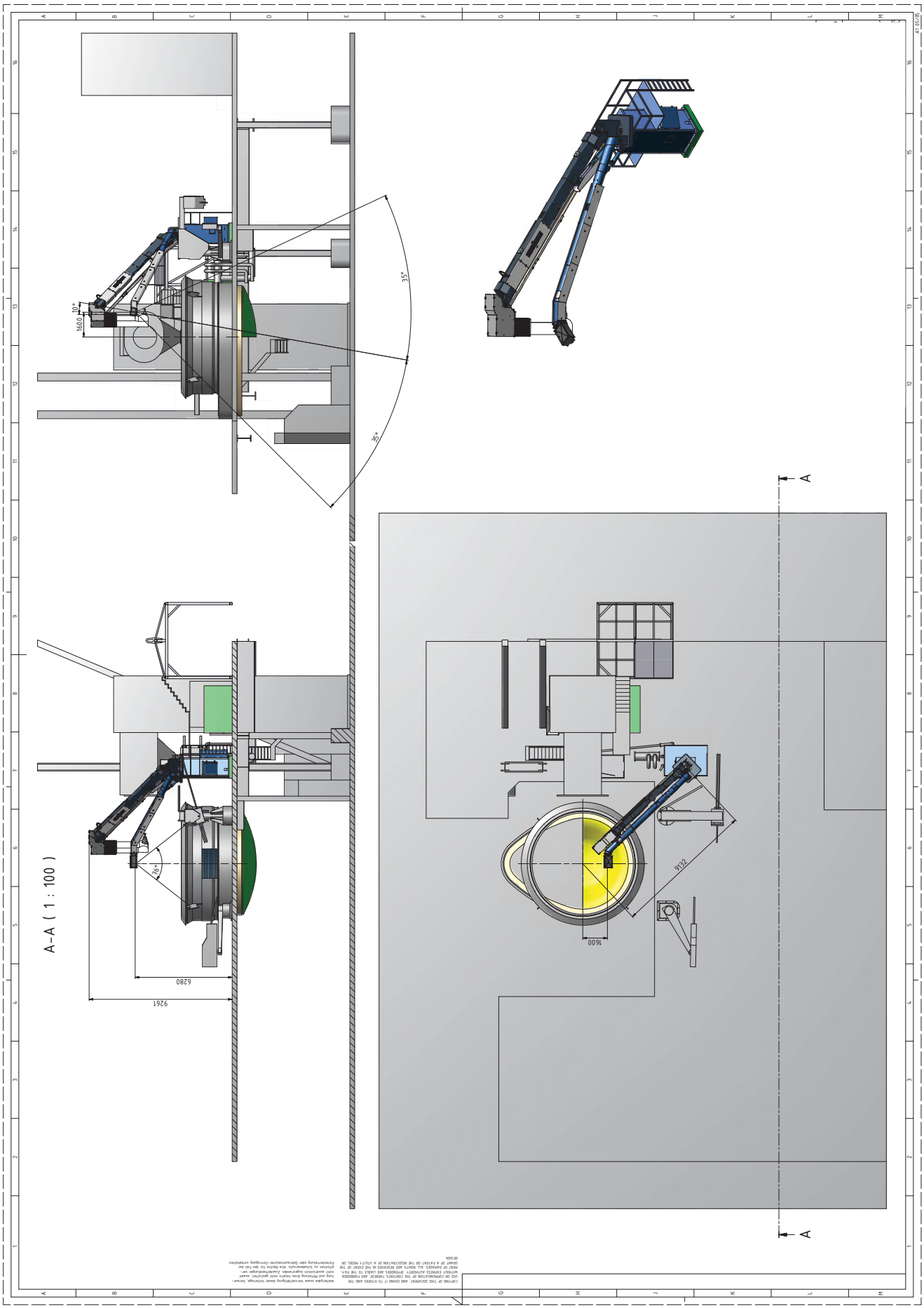

Figure 1.1: Sketch EAF and Terminator. [RHI AG]

1.2 Steelmaking with the Electric Arc Furnace

In an electric arc furnace, see Figure 1.1, batches of molten steel are produced. One such batch melting process is called "heat". A heat includes several operations and is also known as tap to tap cycle. These operations include:

1. Furnace charging
2. Melting
3. Refining
4. De-slagging
5. Tapping
6. Furnace turn-around

1.2.1 Furnace Charging

Generally, before starting a shift, a production plan is made which specifies what grades of steel are going to be produced. Therefore, the scrap yard operator can prepare buckets of scrap and direct reduced iron (DRI) according to the production plan. This is an important step, since it must be ensured that the scrap is layered correctly in the bucket, regarding size and density, to ensure good melting conditions. There are a lot of other considerations to be taken care of, such as making sure no heavy pieces lie directly in front of burner ports to avoid blow-back of the flame onto the water cooler panels and many more.
After carefully preparing the buckets, the first step in a tap to tap cycle is charging the EAF. In order to charge the EAF, the roof and the electrodes are raised and swung to the side. The bucket of scrap and DRI is moved over the furnace with the help of a crane and then the scrap is released into the furnace. Afterwards, the electrodes and the roof are brought back into place.

1.2.2 Melting

The main part of the EAF operations consists of the melting period, also referred to as "Power On Time". By applying electrical or chemical energy to the furnace interior, the melting period is initiated. In case of electrical energy, there exist alternating current (AC) and direct current (DC) furnaces. In AC furnaces usually three graphite electrodes that form an arc between the charged scrap and the electrodes are used to supply the electrical energy. First, a moderate voltage is supplied until the electrodes penetrate the light scrap at the top. This is also known as bore-in phase. The heat to melt the scrap comes from both the current passing through the scrap and the radiation caused by the arc. Following the bore-in phase, in which about 15% of the charged load is melted, high voltage is applied. The high voltage causes longer arcs. The rest of the scrap melts and a pool of liquid metal is formed at the hearth of the furnace. In this phase the arc is considerably stable whereas in the beginning it is rather unstable and large current fluctuations can be detected.

In DC arc furnaces only one electrode is needed at the roof but this setup needs a conductive bottom lining.
One of the most common sources of chemical energy are oxy-fuel burners that burn natural gas using oxygen or a combination of oxygen and air. The heat to melt the scrap comes on the one hand from flame radiation and on the other hand from radiation caused by combustion. Since large pieces of scrap take longer to melt, some operations inject oxygen with a pipe lance to split the large parts into smaller ones. This is caused by the reaction of oxygen with the hot scrap. The injected oxygen also reacts with other elements in the melted bath, which causes additional heat.

The formation of slag on the top of the bath, where metallic oxides and other contaminations are bound, is very important and is induced by admixing so called slag formers. These slag formers come in the form of burnt lime and magnesium oxide and are blown into the furnace during meltdown or are charged with the scrap. Iron oxide, a product that results from steel combustion, is also a component of the EAF slag. An additional but important benefit of the slag is the protection of the EAF roof from intense heat radiation and better arc stability and also results in better energy efficiency. To further improve these slack properties, carbon is added to the slag [2]. Carbon reacts with the iron oxide and results in metallic iron and carbon monoxide. The carbon monoxide causes the slag to foam and improves the thermal shielding and arc stability even more.

Optionally, a second bucket of scrap can be charged by the time the first charge has melted sufficiently. Modern operations tend to charge the furnace only once to reduce heat loss caused by opening the EAF roof and to minimize the tap to tap time. Once the whole scrap is fully melted, a condition is reached that is called flat bath. The melting master can now take samples to decide what actions to take during refining.

1.2.3 Refining

Refining is the operation of removing unwanted elements to achieve the desired steel grade. In the past, refining was performed after the flat bath has been reached. Some of the undesired elements include phosphorus, sulfur, aluminum, silicon, manganese and carbon. Removal of these elements is achieved by blasting oxygen into the bath and adding more slag formers to bind them. To control impurities caused by metals such as copper and nickel, DRI and pig iron has to be introduced.
In modern EAF operations, refining and melting are performed almost simultaneously since the optimal conditions for removing phosphorus and sulfur are conflictive.

1.2.4 De-slagging

Phosphorous is removed best at low temperatures, i.e. at the beginning of a heat. Once the desired amount of phosphorous is bound in the slag, the EAF is tilted and the slag is poured from the furnace through the slag door. Slag also may overflow during the injection of carbon which causes foam as described above. If the sill level in the furnace is reached, the slag can flow out through the slag door.

1.2.5 Tapping

As soon as the desired steel chemistry is reached and the correct temperature is achieved, the steel is poured into a preheated ladle through the taphole. The process of pouring the steel is called tapping.

1.2.6 Furnace Turn-around

Furnace turn-around is the time between tapping and furnace charging. In this time span, the furnace is carefully inspected to discover any defects. The water cooled elements are inspected to detect any possible leaks since the refractory is susceptible to water and more over, leaks can lead to steam explosions. Refractory inspections are also very important because massive wear can lead to breakouts where slag and steel could leak out of the furnace. Therefore, the refractory is maintained regularly. Since maintenance is such a crucial part of securely operating an EAF, this part is usually the largest dead time period in a heat cycle.
Automated maintenance happens mainly in two forms which are called gunning and fettling.

Gunning is a process where refractory material (gunning mix) is applied to the furnace lining in order to counteract the wear. Fettling material is mainly applied to the electric arc furnace bottom and banks. It has quick sintering properties to ensure high durability against slag effects and mechanical wear-out.

1.3 Motivation

Refractory wear is a great concern in the process of steelmaking. Therefore all steelmakers have to face the issue of maintenance tasks. Time used for maintenance is time where no steel is produced which is a cost factor to be optimized. The RHI AG started a project called "Automatische Pflegeprogrammoptimierung" (APO) [3]. The long term goal of APO is to predict the remaining useful life (RUL) of refractory bricks in different steelmaking processes and to propose optimal maintenance. Furthermore, this proposed maintenance should be executed autonomously by a maintenance robot.

Scope of this thesis

To reach the goal of APO this thesis addresses the prediction of the refractory wear. The goal is to predict the refractory wear with the help of a production plan that is known in advance. This production plan contains information about what steel grades are going to be produced. For the prediction of the refractory wear we design and evaluate three linear models that make use of the well-known Kalman filter. The first model heavily relies on the wear rates of the most frequent steel grades which are previously calculated from an overdetermined system of linear equations. The second model is designed for adaption of the wear rate during the lifetime of an EAF but also relies on a modified version of the control inputs. The third model is designed to adapt the wear of the most common steel grades and the maintenance actions separately. A simplified sketch of these models can be seen in Figure 1.2.

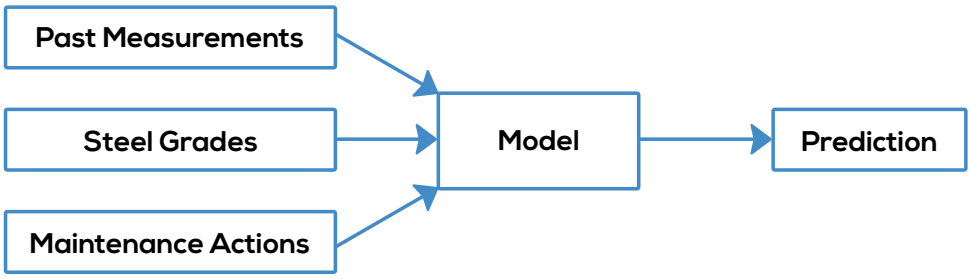

Figure 1.2: Sketch of models in this thesis.

All three models are evaluated individually. We show that all three models promise good prediction results as long as the ground truth data, i.e., the laser measurements are plausible. In a further step, we compare all three models. This comparison leads to the conclusion that the performance of the three models is similarly good, with the exception of Model Two. At average, Model Two has a slightly higher error. We show that all three models are able to predict the wear of the refractory of an EAF.

1.4 Involved Companies

1.4.1 RHI AG

RHI is the world market leader in refractories. The company is a global supplier of high-grade refractory products, systems and services for industrial high-temperature processes that exceed 1200 °C. More than 10000 customers in different industries including steel, cement, glass, nonferrous metals and chemical industries are served by RHI. The RHI headquarters is located in Vienna, Austria and is the purchaser of this thesis.

1.4.2 Emirates Steel

Emirates Steel has been founded in 1998 and is owned by SENAAT, the United Arab Emirates largest industrial conglomerate. Emirates steel is based in Abu Dhabi, U.A.E. and provides all the data discussed in this thesis, namely production data, laser measurements and maintenance data.

1.4.3 Process Metrix

Process Metrix was founded in 1987 and is located in Pleasanton, California. Process Metrix constructs laser and vision based systems for process industries. The laser measurement system and the according software used to acquire the laser measurement data was provided by this company.

2 Theory and Background

Contents

2.1 Least Squares Method 13
2.2 Kalman Filter 15
2.3 Data Set 20
2.3.1 Laser Measurements 20
2.3.2 Production Data 21
2.3.3 Maintenance Data 21
2.3.4 Hot Spots 21

2.1 Least Squares Method

Carl Friedrich Gauss has been attributed with the invention of the least squares method [4]. It was the first attempt to form an optimal estimate from noisy data. Since then, the method of least squares has suited many generations of scientists and still is a useful method to solve an overdetermined system of linear equations. The most common form of a least-squares problem can be written in the form of

$$\begin{bmatrix} h_{11} & h_{12} & h_{13} & \cdots & h_{1n} \\ h_{21} & h_{22} & h_{23} & \cdots & h_{2n} \\ h_{31} & h_{32} & h_{33} & \cdots & h_{3n} \\ \vdots & \vdots & \vdots & \ddots & \vdots \\ h_{l1} & h_{l2} & h_{l3} & \cdots & h_{ln} \end{bmatrix} \begin{bmatrix} x_1 \\ x_2 \\ x_3 \\ \vdots \\ x_n \end{bmatrix} = \begin{bmatrix} z_1 \\ z_2 \\ z_3 \\ \vdots \\ z_l \end{bmatrix}; \tag{2.1}$$

where h_{ln} is the nth feature of sample l, z_l is the target of the lth sample and x_n represents the weight.
Equation 2.1 can be rewritten in matrix notation

$$\mathbf{Hx} = \mathbf{z}, \tag{2.2}$$

where we use uppercase boldface symbols to denote matrices and lowercase boldface symbols to denote vectors. The objective is to find an estimate of the weights $\hat{\mathbf{x}}$ that minimizes the squared estimated measurement error

$$\mathcal{E}^2(\hat{\mathbf{x}}) = |\mathbf{H}\hat{\mathbf{x}} - \mathbf{z}|^2 = \sum_{i=1}^{m} \left[\sum_{j=1}^{n} h_{ij}\hat{x_j} - z_i \right]^2. \tag{2.3}$$

As generally known, to find $\hat{\mathbf{x}}$ minimizing an equation $\mathcal{E}(\hat{\mathbf{x}})$, i.e. $\text{argmin}_x = \mathcal{E}(\hat{\mathbf{x}})$, one can use gradient descent techniques. In this case of a convex objective, the minimum is found where the

first derivative is zero, i.e.

$$\frac{\delta \mathcal{E}^2(\hat{\mathbf{x}})}{\delta \hat{x_k}} \stackrel{!}{=} 0 \tag{2.4}$$

for $k = 1, 2, 3, \ldots, n$. Setting the derivative of Equation 2.3 to zero leads to

$$\frac{\delta \mathcal{E}^2(\hat{\mathbf{x}})}{\delta \hat{x_k}} = 2 \sum_{i=1}^{m} h_{ik} \sum_{j=1}^{n} h_{ij} \hat{x}_j - z_i \stackrel{!}{=} 0 \tag{2.5}$$

which can be rewritten in matrix notation as follows

$$2\mathbf{H}^T[\mathbf{H}\hat{\mathbf{x}} - \mathbf{z}] \stackrel{!}{=} 0 \tag{2.6}$$

and

$$\mathbf{H}^T\mathbf{H}\hat{\mathbf{x}} = \mathbf{H}^T\mathbf{z}. \tag{2.7}$$

Equation 2.7 is known as the *normal form of the equation for the linear least-squares problem* and has exactly as many scalar equations as unknowns.
The solution for the estimation of $\hat{\mathbf{x}}$ is

$$\hat{\mathbf{x}} = (\mathbf{H}^T\mathbf{H})^{-1}\mathbf{H}^T\mathbf{z} \tag{2.8}$$

as long as the matrix product $\mathcal{G} = \mathbf{H}^T\mathbf{H}$ is nonsingular, $\mathcal{G}$ is invertible. $\mathcal{G}$ is called the Gramian matrix and its determinant defines whether $\hat{\mathbf{x}}$ has a unique solution:

$$\det(\mathcal{G}) = \begin{cases} 0 & \text{no unique solution} \\ \text{otherwise} & \text{unique solution} \end{cases} \tag{2.9}$$

2.2 Kalman Filter

The Kalman filter, developed by Rudlf E. Kalman [5] in 1960, is used in a wide field of engineering approaches and is clearly established as a fundamental tool for analyzing and solving a broad range of estimation and filtering problems. Probably the most famous application to date was the use of the Kalman filter in the Apollo mission to the moon [6]. More recent applications include global positioning receivers, output smoothing of mouse trackpads, tracking objects, fusing data from different sensors and many more [7]. Generally, the application of this filter is to estimate a process state at some given point in time and correct this estimation with the help of a feedback. This feedback is a noisy measurement, obtained by a sensor. Therefore the Kalman filter can be seen as a predictor-corrector algorithm [8] [9]. The Kalman filter consists of two parts: the time update which is also known as prediction step and the measurement update also known as correction step. The Kalman filter is a set of mathematical equations that minimize the mean of the squared error of the state estimate of a process. This set of equations provides a recursive solution to the estimation problem since the current predicted step is dependent on the previous estimate and the current input data. For the derivation of the Kalman filter we will take a look at discrete linear dynamical systems, i.e. the observed signals are equally spaced in time. The derivation follows closely the steps discussed in [10]. The process equation of such a discrete linear system is defined by

$$\mathbf{x}_{k+1} = \mathbf{F}_{k+1}\mathbf{x}_k + \mathbf{w}_k, \tag{2.10}$$

where $\mathbf{F}_{k+1}$ represents the state transition matrix that propagates the state vector from $\mathbf{x}_k$ to $\mathbf{x}_{k+1}$, at time step k. The vector $\mathbf{w}_k$ is the process noise, assumed to be white, additive and Gaussian with zero mean, where

$$E[\mathbf{w}_n\mathbf{w}_k^T] = \begin{cases} \mathbf{Q}_k & \text{for } n = k \\ \mathbf{0} & \text{for } n \neq k, \end{cases} \tag{2.11}$$

is the covariance matrix $\mathbf{Q}_k$ of the process noise. The state $\mathbf{x}_{k+1}$ is unknown and needs to be estimated for $\mathbf{x}_k$. A second equation is needed for an observation $\mathbf{y}_k$. This equation is called the measurement equation and is defined by

$$\mathbf{y}_k = \mathbf{H}_k\mathbf{x}_k + \mathbf{v}_k, \tag{2.12}$$

with $\mathbf{v}_k$ being the measurement noise vector which is also assumed to be white, and Gaussian with zero mean. The covariance matrix for the measurement noise is described by

$$E[\mathbf{v}_n\mathbf{v}_k^T] = \begin{cases} \mathbf{R}_k & \text{for } n = k \\ \mathbf{0} & \text{for } n \neq k. \end{cases} \tag{2.13}$$

The same assumptions as for the process noise apply to the measurement noise. Additionally it is assumed that the measurement noise is uncorrelated with the process noise.
With these definitions in mind, the Kalman filtering problem can be formulated as finding the minimum mean squared error for the state estimate $\mathbf{x}_i$ using all observed data $\mathbf{y}_1, \mathbf{y}_2, \ldots, \mathbf{y}_k$ known at time k. If $k = i$, the above defined problem is called filtering. If $i > k$, it is called prediction and if $1 <= i < k$, the problem is known as Kalman smoothing.
Before delving into the derivation a few additional equations have to be defined. First, the equation

$$\mathbf{y}_k = \mathbf{x}_k + \mathbf{v}_k \tag{2.14}$$

defines the observable $\mathbf{y}_k$ and the unknown signal $\mathbf{x}_k$ at a given point k in time. Considering all observations $\mathbf{y}_1, \mathbf{y}_2, \ldots, \mathbf{y}_k$, the a posteriori estimate of $\mathbf{x}_k$ is defined by $\hat{\mathbf{x}}_k$. Since $\hat{\mathbf{x}}_k$ is an estimate, it is likely to be different from the true unknown signal $\mathbf{x}_k$. Therefore, the mean squared error as a cost function is defined as

$$\mathbf{J}_k = \mathcal{E}[\tilde{\mathbf{x}}_k^2], \tag{2.15}$$

where $\tilde{\mathbf{x}}_k$ is the estimation error defined by

$$\tilde{\mathbf{x}}_k = \mathbf{x}_k - \hat{\mathbf{x}}_\mathbf{k}. \tag{2.16}$$

In order to find the optimal estimate of $\hat{\mathbf{x}}_k$, two theorems need to be formulated [11] which are restated from [10]:

Theorem 1.1 Conditional mean estimator

If the stochastic processes $\mathbf{x}_1, \mathbf{x}_2, \ldots, \mathbf{x}_k$ and $\mathbf{y}_1, \mathbf{y}_2, \ldots, \mathbf{y}_k$ are jointly Gaussian, the optimum estimate $\hat{\mathbf{x}}_k$ that minimizes the mean-square error $\mathbf{J}_k$ is the conditional mean estimator

$$\hat{\mathbf{x}}_k = E[\mathbf{x}_k | \mathbf{y}_1,\ \mathbf{y}_2,\ ...,\ \mathbf{y}_k], \tag{2.17}$$

where $E[.]$ denotes the expectation.

Theorem 1.2 Principle of orthogonality

Let the stochastic processes $\mathbf{x}_k$ and $\mathbf{y}_k$ be of zero means; that is,

$$E[\mathbf{x}_k] = E[\mathbf{y}_k] = 0 \quad \text{for all } k. \tag{2.18}$$

Then:

- the stochastic processes $\mathbf{x}_1, \mathbf{x}_2, \ldots, \mathbf{x}_k$ and $\mathbf{y}_1, \mathbf{y}_2, \ldots, \mathbf{y}_k$ are jointly Gaussian; or
- if the optimal estimate $\hat{\mathbf{x}}_k$ is restricted to be a linear function of the observables and the cost function is the mean-square error;
- then the optimum estimate $\hat{\mathbf{x}}_k$, given the observables $\mathbf{y}_1, \mathbf{y}_2, \ldots, \mathbf{y}_k$, is the orthogonal projection of $\mathbf{x}_k$ on the space spanned by these observables.

When we get a new measurement $\mathbf{y}_k$ at time k for the dynamic linear system we defined in 2.10 and 2.12, we want to use the new measurement in the new estimate of $\hat{\mathbf{x}}_\mathbf{k}$ with

$$\hat{\mathbf{x}}_k = \mathbf{G}_k^{(1)} \hat{\mathbf{x}}_k^- + \mathbf{G}_k \mathbf{y}_k, \tag{2.19}$$

where $\hat{\mathbf{x}}^-$ describes the a priori estimate that is already known at time k and where the matrices $\mathbf{G}_k^{(1)}$ and $\mathbf{G}_k$ are yet unknown and need to be determined. Now, Theorem 1.2 is used:

$$E[\tilde{\mathbf{x}}_k \mathbf{y}_i^T] = \mathbf{0} \quad \text{for } i = 1, 2, ..., k-1 \tag{2.20}$$

Substituting Equations 2.12, 2.16 and 2.19 into 2.20 leads to

$$E[(\mathbf{x}_k - \mathbf{G}_k^{(1)} \hat{\mathbf{x}}_k^- - \mathbf{G}_k \mathbf{H}_k \mathbf{x}_k - \mathbf{G}_k \mathbf{v}_k) \mathbf{y}_i^T] = \mathbf{0} \quad \text{for } i = 1, 2, \ldots, k-1. \tag{2.21}$$

As stated earlier, the measurement and the measurement noise are uncorrelated, i.e.

$$E[\mathbf{v}_k \mathbf{y}_k^T] = \mathbf{0}. \tag{2.22}$$

Applying 2.22 to 2.21 and reorganizing the terms results in

$$E[(\mathbf{I} - \mathbf{G}_k\mathbf{H}_k - \mathbf{G}_k^{(1)})\mathbf{x}_k\mathbf{y}_i^T + \mathbf{G}_k^{(1)}(\mathbf{x}_k - \hat{\mathbf{x}}_k^-)\mathbf{y}_i^T] = \mathbf{0}, \tag{2.23}$$

where $\mathbf{I}$ is the identity matrix. Since the state vector $\mathbf{x}_k$ and the observable $\mathbf{y}_i$ are orthogonal, one can say that the estimate and the observable are also orthogonal. Therefore, the state error vector and the observable are orthogonal, too, i.e.

$$E[(\mathbf{x}_k - \hat{\mathbf{x}}_k^-)\mathbf{y}_i^T] = \mathbf{0}. \tag{2.24}$$

Using 2.24 in 2.23 leads to

$$(\mathbf{I} - \mathbf{G}_k\mathbf{H}_k - \mathbf{G}_k^{(1)})E[\mathbf{x}_k\mathbf{y}_i^T] = \mathbf{0} \quad \text{for } i = 1, 2, ..., k-1. \tag{2.25}$$

For arbitrary values of $\mathbf{x}_k$ and $\mathbf{y}_i$, Equation 2.25 holds if

$$\mathbf{G}^{(1)} = \mathbf{I} - \mathbf{G}_k\mathbf{H}_k. \tag{2.26}$$

The a priori estimate $\hat{\mathbf{x}}_k$ was defined in Equation 2.19. The matrix $\mathbf{G}^{(1)}$ can now be substituted with Equation 2.26 as follows

$$\hat{\mathbf{x}}_k = \hat{\mathbf{x}}_k^- + \mathbf{G}_k(\mathbf{y}_k - \mathbf{H}_k\hat{\mathbf{x}}_k^-), \tag{2.27}$$

which is also known as the state estimation update equation.
In the next step, an equation needs to be found to calculate the Kalman gain $\mathbf{G}_k$. Again, the orthogonality principle from Theorem 1.2 can be used, i.e.,

$$E[(\mathbf{x}_k - \hat{\mathbf{x}}_k)\mathbf{y}_k^T] = \mathbf{0}. \tag{2.28}$$

Since $\hat{\mathbf{y}}_k^T$ is the estimate of $\mathbf{y}_k^T$ Equation 2.28 can be rewritten as

$$E[(\mathbf{x}_k - \hat{\mathbf{x}}_k)\hat{\mathbf{y}}_k^T] = \mathbf{0}. \tag{2.29}$$

The residual of the real and estimated observation, also called the innovation process, is defined by

$$\tilde{\mathbf{y}}_k = \mathbf{y}_k - \hat{\mathbf{y}}_k \tag{2.30}$$

In Equation 2.12 $\mathbf{y}_k$ was defined. Therefore, Equation 2.30 can be reformulated as

$$\begin{aligned}\tilde{\mathbf{y}}_k &= \mathbf{H}_k\mathbf{x}_k + \mathbf{v}_k - \mathbf{H}_k\hat{\mathbf{x}}_k^- \\ &= \mathbf{H}_k\tilde{\mathbf{x}}_k^- + \mathbf{v}_k.\end{aligned} \tag{2.31}$$

With the help of Equation 2.12 and 2.27 the equation for the state error vector can be defined as

$$\begin{aligned}\mathbf{x}_k - \hat{\mathbf{x}}_k &= \tilde{\mathbf{x}}_k^- - \mathbf{G}_k(\mathbf{H}_k\tilde{\mathbf{x}}_k + \mathbf{v_k}) \\ &= (\mathbf{I} - \mathbf{G}_k\mathbf{H}_k)\tilde{\mathbf{x}}_k^- - \mathbf{G}_k\mathbf{v}_k.\end{aligned} \tag{2.32}$$

With Equation 2.31 and 2.32 at hand, Equation 2.29 can be rewritten as

$$E[\{\mathbf{I} - \mathbf{G}_k\mathbf{H}_k)\tilde{\mathbf{x}}_k^- - \mathbf{G}_k\mathbf{v}_k\}(\mathbf{H}_k\tilde{\mathbf{x}}_k^- + \mathbf{v}_k)] = \mathbf{0}. \tag{2.33}$$

Knowing that the state error $\tilde{\mathbf{x}}_k^-$ and the measurement noise $\mathbf{v}_k$ are independent, Theorem 1.2 can be invoked. This results in the simplification of Equation 2.33

$$(\mathbf{I} - \mathbf{G}_k\mathbf{H}_k)\underbrace{E[\tilde{\mathbf{x}}_k\tilde{\mathbf{x}}_k^{T-}]}_{\mathbf{P}_k^-}\mathbf{H}_k^T - \mathbf{G}_k\underbrace{E[\mathbf{v}_k\mathbf{v}_k^T]}_{\mathbf{R}_k} = \mathbf{0}, \tag{2.34}$$

where $\mathbf{P}_k^-$ is the a priori covariance matrix of the state error vector

$$\begin{aligned}\mathbf{P}_k^- &= E[(\mathbf{x}_k - \hat{\mathbf{x}}_k^-)(\mathbf{x}_k - \hat{\mathbf{x}}_k^-)^T] \\ &= E[\tilde{\mathbf{x}}_k^-\tilde{\mathbf{x}}_k^{T-}]\end{aligned} \tag{2.35}$$

and $\mathbf{R}_k$ is the covariance matrix of the measurement noise defined in 2.13. Substituting these matrices and solving for $\mathbf{G}_k$ leads to the formula for the Kalman gain matrix

$$\mathbf{G}_k = \mathbf{P}_k^-\mathbf{H}_k^T[\mathbf{H}_k\mathbf{P}_k^-\mathbf{H}_k^T + \mathbf{R}_k]^{-1}. \tag{2.36}$$

The last steps in deriving the Kalman filter equations are to determine the formulas for the error covariance propagation. As stated in [10], this propagation involves two steps.

- The a priori covariance matrix $\mathbf{P}_k^-$ was already defined in 2.35. With the a priori covariance at hand, the a posteriori covariance matrix $\mathbf{P}_k$ at time k is determined as

$$\begin{aligned}\mathbf{P}_k &= E[(\tilde{\mathbf{x}}_k\mathbf{x}_k^T] \\ &= E[\mathbf{x}_k - \hat{\mathbf{x}}_k)(\mathbf{x}_k - \hat{\mathbf{x}}_k)^T].\end{aligned} \tag{2.37}$$

- With the help of the a posteriori covariance matrix $\mathbf{P}_{k-1}$ of the previous time step $k-1$ the new a priori covariance matrix $\mathbf{P}_k^-$ needs to be calculated.

Starting with the first step, Equation 2.32 can be combined with 2.37 which results in

$$\begin{aligned}\mathbf{P}_k &= E[\{(\mathbf{I} - \mathbf{G}_k\mathbf{H}_k)\tilde{\mathbf{x}}_k^- - \mathbf{G}_k\mathbf{v}_k\}\{(\mathbf{I} - \mathbf{G}_k\mathbf{H}_k)\tilde{\mathbf{x}}_k^- - \mathbf{G}_k\mathbf{v}_k\}^T] \\ &= E[(\mathbf{I} - \mathbf{G}_k\mathbf{H}_k)\tilde{\mathbf{x}}_k^-\tilde{\mathbf{x}}_k^{T-}(\mathbf{I} - \mathbf{G}_k\mathbf{H}_k)^T - \underbrace{(\mathbf{I} - \mathbf{G}_k\mathbf{H}_k)\tilde{\mathbf{x}}_k^-\mathbf{v}_k^T\mathbf{G}_k^T}_{\mathbf{0}} \\ &\quad - \underbrace{\tilde{\mathbf{x}}^{T-}(\mathbf{I} - \mathbf{G}_k\mathbf{H}_k)^T\mathbf{G}_k\mathbf{v}_k}_{\mathbf{0}} + \mathbf{G}_k\mathbf{v}_k\mathbf{v}_k^T\mathbf{G}_k^T] \\ &= (\mathbf{I} - \mathbf{G}_k\mathbf{H}_k)\underbrace{E[\tilde{\mathbf{x}}_k^-\tilde{\mathbf{x}}_k^{T-}]}_{\mathbf{P}_\mathbf{k}^-}(\mathbf{I} - \mathbf{G}_k\mathbf{H}_k)^T + \mathbf{G}_k\underbrace{E[\mathbf{v}_k\mathbf{v}_k^T]}_{\mathbf{R}_k}\mathbf{G}_k^T \\ &= (\mathbf{I} - \mathbf{G}_k\mathbf{H}_k)\mathbf{P}_k^-(\mathbf{I} - \mathbf{G}_k\mathbf{H}_k)^T + \mathbf{G}_k\mathbf{R}_k\mathbf{G}_k^T \\ &= (\mathbf{I} - \mathbf{G}_k\mathbf{H}_k)\mathbf{P}_k^- - \underbrace{(\mathbf{I} - \mathbf{G}_k\mathbf{H}_k)\mathbf{P}_k^-\mathbf{H}_k^T}_{\mathbf{G}_k\mathbf{R}_k}\mathbf{G}_k^T + \mathbf{G}_k\mathbf{R}_k\mathbf{G}_k^T \\ &= (\mathbf{I} - \mathbf{G}_k\mathbf{H}_k)\mathbf{P}_k^- - \mathbf{G}_k\mathbf{R}_k\mathbf{G}_k^T + \mathbf{G}_k\mathbf{R}_k\mathbf{G}_k^T \\ &= (\mathbf{I} - \mathbf{G}_k\mathbf{H}_k)\mathbf{P}_k^-.\end{aligned} \tag{2.38, 2.39, 2.40}$$

In 2.38 Theorem 1.2 is used, since it is assumed that the measurement noise and the a priori estimation error are independent and therefore the two middle terms are zero. In 2.39 one can recognize the term from Equation 2.34. Equation 2.40 is the resulting formula for the error covariance update. We can then proceed to derive the last equation needed for the Kalman filter which is the error covariance propagation. Since the a priori estimate is propagated through time and therefore depends on the estimate of the time step before, it follows that

$$\hat{\mathbf{x}}_k^- = \mathbf{F}_{k,k-1}\hat{\mathbf{x}}_{k-1}. \tag{2.41}$$

The a priori estimation error can be rewritten using Equations 2.10 and 2.41 as

$$\begin{aligned}\tilde{\mathbf{x}}_k^- &= \mathbf{x}_k - \hat{\mathbf{x}}_k^- \\ &= (\mathbf{F}_k\mathbf{x}_{k-1} + \mathbf{w}_{k-1}) - (\mathbf{F}_k\hat{\mathbf{x}}_{k-1}) \\ &= \mathbf{F}_k(\mathbf{x_{k-1}} - \hat{\mathbf{x}}_{k-1}) + \mathbf{w}_{k-1} \\ &= \mathbf{F}_k\tilde{\mathbf{x}}_{k-1} + \mathbf{w}_{k-1}. \end{aligned} \tag{2.42}$$

Equation 2.42 can be substituted into 2.35 by applying the orthogonality principle stated in Theorem 1.2, since the process noise and the state error vector are independent. Thus we obtain

$$\begin{aligned}\mathbf{P}_k^- &= E[\tilde{\mathbf{x}}_k^-\tilde{\mathbf{x}}_k^{T-}] \\ &= E[\mathbf{F}_k\tilde{\mathbf{x}}_{k-1}\tilde{\mathbf{x}}_{k-1}^T\mathbf{F}_k^T + \underbrace{\mathbf{F}_k\tilde{\mathbf{x}}_{k-1}\mathbf{w}_{k-1}^T}_{\mathbf{0}} + \underbrace{\mathbf{w}_{k-1}\mathbf{F}_k^T\tilde{\mathbf{x}}_{k-1}^T}_{\mathbf{0}} + \mathbf{w}_{k-1}\mathbf{w}_{k-1}^T] \\ &= \mathbf{F}_k \underbrace{E[\tilde{\mathbf{x}}_{k-1}\tilde{\mathbf{x}}_{k-1}^T]}_{\mathbf{P}_{k-1}}\mathbf{F}_k^T + \underbrace{E[\mathbf{w}_{k-1}\mathbf{w}_{k-1}^T]}_{\mathbf{Q}_{k-1}} \\ &= \mathbf{F}_k\mathbf{P}_{k-1}\mathbf{F}_k^T + \mathbf{Q}_{k-1}. \end{aligned} \tag{2.43}$$

With the error covariance propagation all equations for the Kalman filter are at hand. In general, the Kalman filter consists of two parts, the time update which is called the prediction step and the measurement update called the correction step. Figure 2.1 shows a sketch of this concept. The notation slightly differs from the previous notation, but we refer to the corresponding equations. For the projection to the next time step we additionally add the term $\mathbf{B}\mathbf{u}_k$ where $\mathbf{u}_k$ is an input control vector and $\mathbf{B}$ is an input control model.

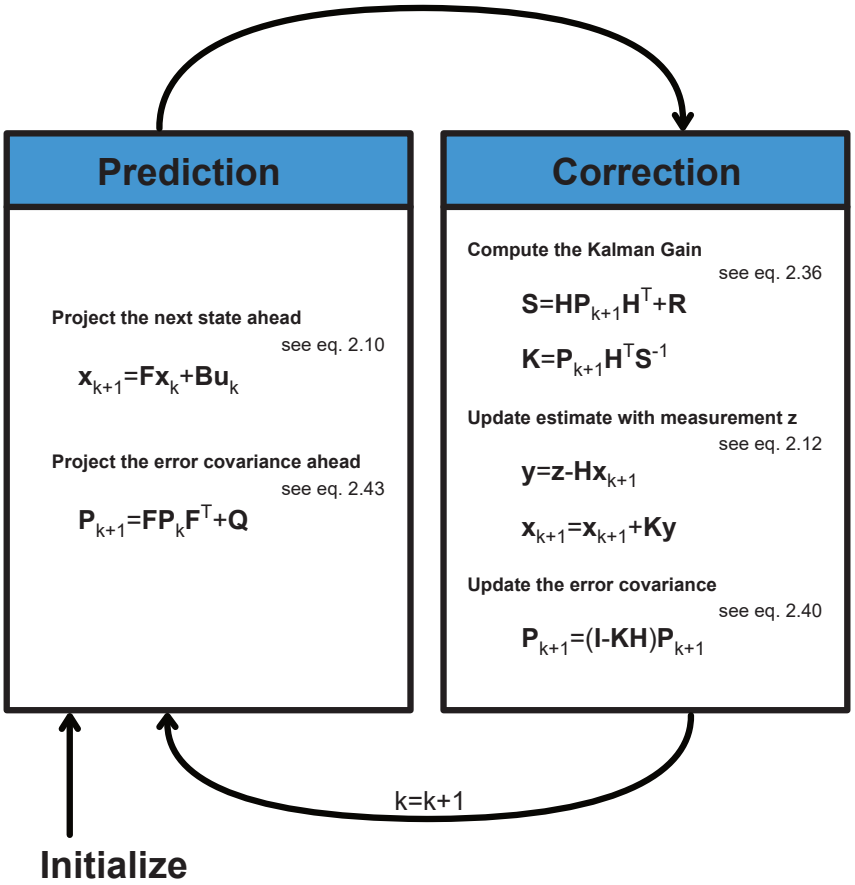

Figure 2.1: Sketch of prediction-correction process.

2.3 Data Set

The data set is structured into individual campaigns. One campaign represents the lifetime of an EAF refractory lining. Each campaign consists of several hundred heats. The data set provided for this thesis contains laser measurement data, production parameters and the produced steel grades. Furthermore, maintenance data is available. The data set contains 52 campaigns. Only the last 22 campaigns contain laser measurement data and are therefore used in this thesis.

2.3.1 Laser Measurements

Laser measurements are a crucial part of the steelmaking process. It helps the operator to investigate the condition of the furnace. Since the furnace condition decreases with an increasing number of heats, laser measurements taken at the beginning of a campaign are more sparse than at the end. Laser measurements are taken with a Terminator XL maintenance robot which is a state of the art RHI product for highly efficient gunning repair [12]. The Terminator XL has one arm for gunning and another arm for laser measurements, as can be seen in Figure 2.2. The roof of the EAF has to be opened and then the arm of the Terminator XL is lowered from the top into the EAF to take laser measurements. Opening the roof of the EAF means heat and energy loss. Therefore it is crucial that measurements are taken quickly which leads to significant errors and noise in the measurements. Another big source of error is the positioning of the laser itself. The resulting data is continuous and consists of depth, angle and radius values. The depth values describe how deep the laser is lowered into the furnace, while the radius describes the distance between the laser and the refractory bricks. The angle values describe the radial orientation. From these three values 3D positions can be reconstructed.
This continuous data needs to be processed and cleaned to acquire a uniform, discrete grid of measurement data. Forrer [13] did intensive research on this topic and the data used in this thesis is already processed and cleaned. Preprocessing and cleaning includes interpolating the measurements provided by the laser and taking care of duplicates to achieve an uniform grid of measurement data. Moreover, an attempt has been made to detect outliers.

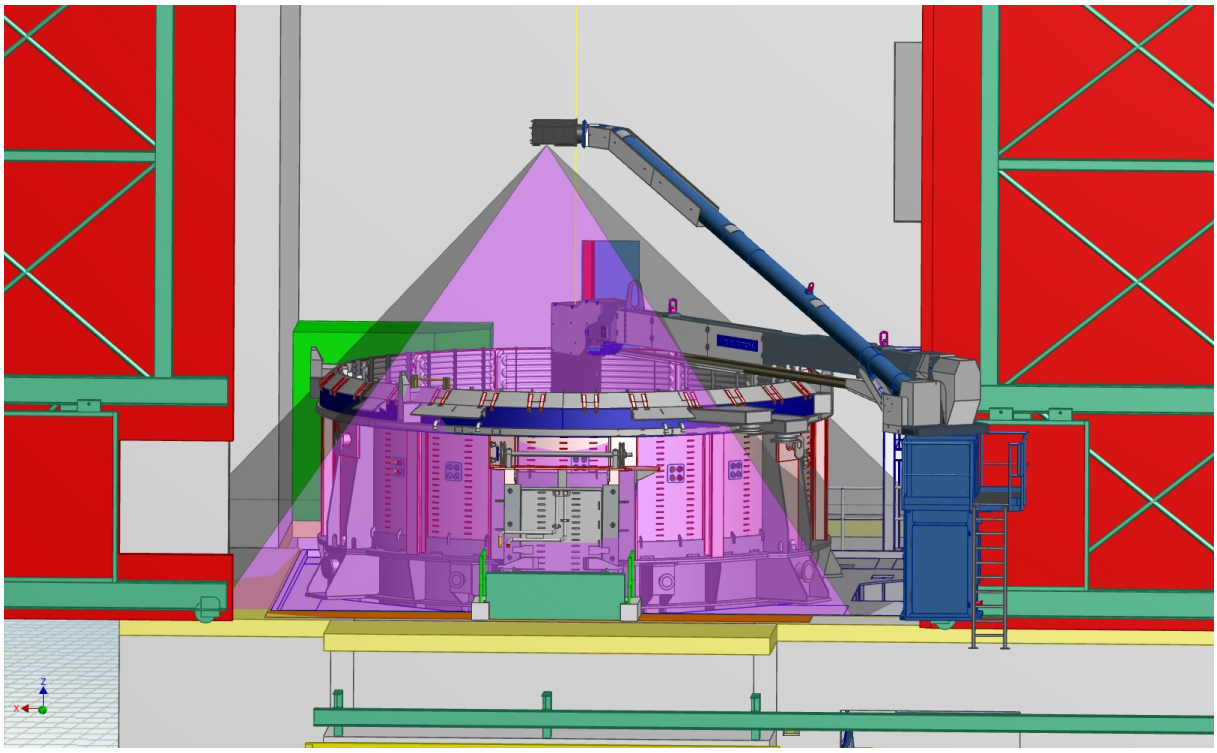

Figure 2.2: Terminator during laser measurement. [RHI AG]

2.3.2 Production Data

Different steel grades are produced following specific "recipes". Depending on the quality of the steel, various elements need to be extracted from the molten bath as described in the steel-making process in Section 1.2. There are about 140 production parameters available, including production time, charged scrap, pig iron, etc. These parameters are available for each heat but are not known in advance and therefore disregarded for this work.

2.3.3 Maintenance Data

Maintenance data is also available but maintenance does not occur periodically. This data describes what actions are taken during maintenance. These actions include gunning and fettling and how much maintenance material has been consumed. Furthermore, the area where the maintenance happened and the duration of the maintenance has been recorded. This data has also been recorded by the Terminator XL. Therefore, maintenance performed by hand is not reflected in the data set. In earlier campaigns, the mapping of the maintenance consumption to a specified area was wrong and only a few campaigns exist with properly mapped maintenance data.

2.3.4 Hot Spots

An EAF is huge in terms of size and dimension. The arrangement of the graphite electrodes influences the areas where the most wear occurs. Specialists from RHI AG have defined so-called "Hot Spots". In our dataset, three Hot Spots have been defined, namely "Hot Spot 1", "Hot Spot 2" and "Slag Door". These Hot Spots describe areas with excessive wear and draw our attention since these areas are prone to breakouts of the liquid steel. Our main research in this thesis has been done on "Hot Spot 1" but is applicable to all of them. Figure 2.3 shows a three-dimensional model constructed from laser data with the definition of Hot Spot 1. Figure 2.4 shows the same Hot Spot in a two-dimensional representation.

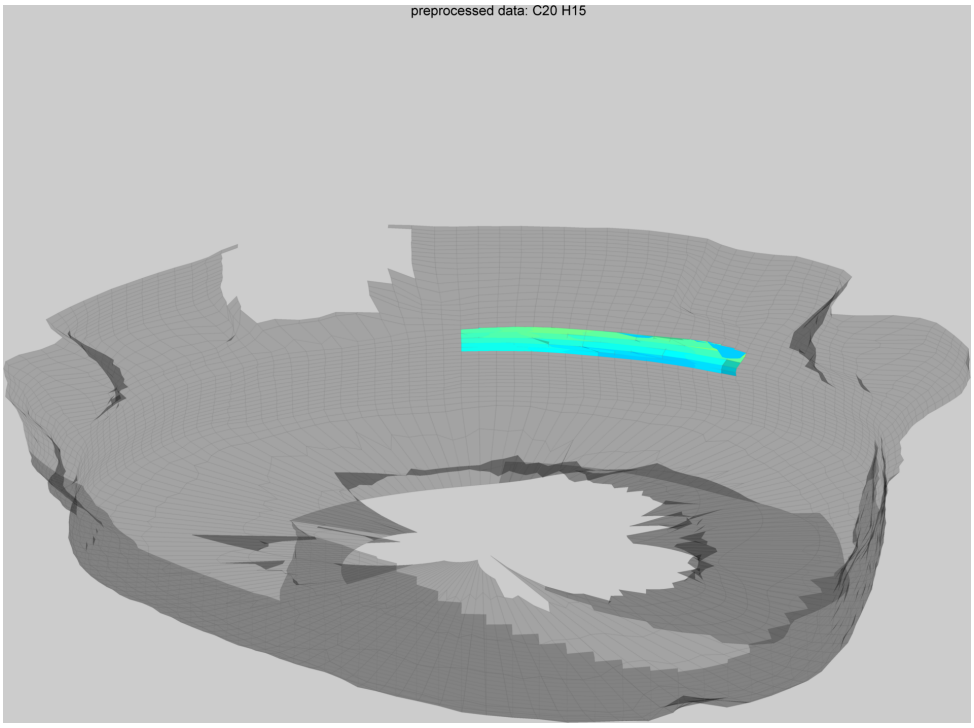

Figure 2.3: 3D view generated from laser measurements. The highlighted area indicates Hot Spot 1

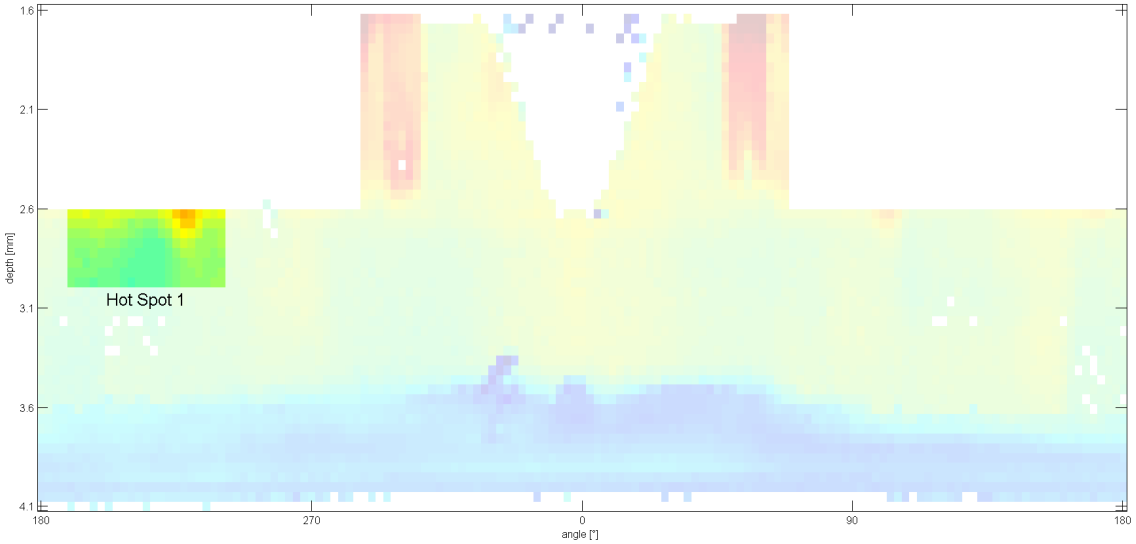

Figure 2.4: 2D view of the laser measurements with Hot Spot 1 highlighted.

3
Approach and Implementation

Contents

3.1 Least Squares Model 24
3.1.1 Approach 24
3.1.2 Implementation 24
3.2 Kalman Filter - Model One 26
3.2.1 Approach 26
3.2.2 Implementation 27
3.3 Kalman Filter - Model Two 28
3.3.1 Approach 28
3.3.2 Implementation 29
3.4 Kalman Filter - Model Three 30
3.4.1 Approach 30
3.4.2 Implementation 31

The main interest of this thesis is to estimate the remaining useful life of an EAF. In other words, we want to estimate the refractory wear for a given Hot Spot in an EAF. The objective is that the estimate is only dependent on as little production parameters as possible and that, according to a given production plan, the expected wear over the course of several heats can be estimated. There is little knowledge about the wear process that is going on in an EAF. The hot, dirty and steamy conditions make it hard to observe the processes that cause wear and tear. Furthermore, the influence of automatic maintenance actions are not clear. We do know that maintenance increases the lifetime of an EAF but we do not know how the maintenance material behaves precisely. In this thesis we try to approximate these processes with linear systems.
From previous research done for BOF [13] we know that different steel grades induce different grades of wear of the refractory material. The steel plant operators try to compensate this wear process with maintenance, especially with gunning and fettling. Therefore an obvious choice for the parameter set used for a prediction model are the steel grades that have been and are going to be produced as well as the maintenance data.

This chapter describes the different models and points out specific implementation details. The development language of our choice is Python 3.5 [14]. Python is an open source programming language which has significantly emerged in the scientific community over the last years. Python has a lot of scientific packages including Numpy [15], which is a highly efficient linear algebra package and Matplotlib [16], which provides a very customizable plotting environment. SciPy [15] is a scientific computing package that provides several numerical algorithms, including optimization, statistics, signal processing and more. We start with a least squares model in Section 3.1 and than proceed to different models using the linear Kalman filter in Sections 3.2 - 3.4.

3.1 Least Squares Model

3.1.1 Approach

As previously described in 2.3.4, three areas have been defined that are exposed to excessive refractory wear. Let us first introduce the term *slot*. A slot defines the timespan between two consecutive laser measurements. In other words, a laser measurement LM_t defines the beginning of a slot and a laser measurement LM_{t+1} defines the end. This concept is depicted in the sketch in Figure 3.1. Each slot can consist of a different timespan since laser measurements don't happen in regular intervals. Obviously, it is possible that in a given slot several different steel grades are produced. Furthermore, one or more maintenance actions could have taken place but maintenance is not mandatory.

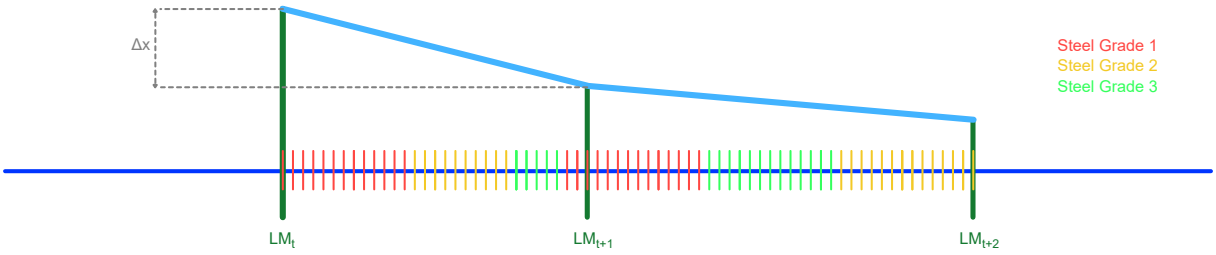

Figure 3.1: Sketch of laser measurement and steel grades.

With these definitions at hand we are able to construct our first model. It is a straight forward linear model. We determine a separate weight for the wear for each steel grade and also consider the maintenance actions as a factor. The provided data set for the steel plant "SMP 1" contains 29 different steel grades that are produced. Some of them are produced seldomly while other steel grades dominate the production plan. We chose to only calculate separate weights for steel grades that have been produced more than 400 times counted over the whole data set. All the other steel grades are collected in a common weight called "others". To estimate these weights, the following system of equations

$$\begin{bmatrix} SG_{1,1} & SG_{1,2} & \cdots & SG_{1,n} & GC_1 \\ SG_{2,1} & SG_{2,2} & \cdots & SG_{2,n} & GC_2 \\ \vdots & \vdots & \ddots & \vdots & \vdots \\ SG_{m,1} & SG_{m,2} & \cdots & SG_{m,n} & GC_m \end{bmatrix} \begin{bmatrix} w_1 \\ w_2 \\ \vdots \\ w_{n+1} \end{bmatrix} = \begin{bmatrix} \Delta x_1 \\ \Delta x_2 \\ \vdots \\ \Delta x_m \end{bmatrix} \tag{3.1}$$

is used. Each line of this equation system is populated from one slot. The variables $SG_1, \ldots, SG_n$ represent the frequency count of how often a specific steel grade has been produced in a given slot. The automatic maintenance actions, e.g. gunning, are represented with the variable GC which represents the frequency count of the gunning actions. Δx holds the wear of the refractory lining that occurred in a given slot. To solve this overdetermined system for the weights $w_1, \ldots, w_{n+1}$, the method of least squares introduced in Section 2.1 is used.

3.1.2 Implementation

The practical implementation in Python 3.5 uses the numpy and scipy.opitmize packages. SciPy provides a curve fit function which needs at least three arguments. These three arguments consist of a function to be minimized and the parameters `xdata` and `ydata`. The `xdata` variable in this case is the steel grade matrix as discussed above and the `ydata` variable is an array with the corresponding wear values. Amongst other optional arguments, one is to provide an initial guess of the coefficients. We initialize these coefficients with ones. The result of the `curve_fit`

function is the least squares solution of Equation 3.1. Listing 1 shows an excerpt from the practical implementation.

```
import numpy as np
import scipy.optimize as spo

def fit_func(x, *p):
    a = np.array(x)
    b = np.array(p)
    return np.dot(b, a)

def linear_fit(x, y, p):
    err = 0
    coeff = []

    try:
        coeff, var_matrix = spo.curve_fit(fit_func, x, y, p0=p)
    except RuntimeError:
        err = 1
        print("Fitting Error")
    return coeff, err

startCoeff = [1.0 for c in range(0, len(lHeatFamiliesLimited) + 1)]
coeff, err = linear_fit(npSteelgrade, npDeltas, startCoeff)
```

Listing 1: Excerpt of the least squares implementation.

3.2 Kalman Filter - Model One

3.2.1 Approach

The first model designed is a one-dimensional linear Kalman filter with control inputs $\mathbf{u}_k$. We stick to boldface symbols for vectors and matrices although in this model they are scalar values. The equations for the prediction step and respectively for the update step are listed in 3.2 and 3.3. The first part of the filter equation consists of a scalar $\mathbf{x}_k$, representing the remaining depth of the refractory bricks. The subscript k defines the step number in time in terms of the produced heats. The state transition matrix is also a scalar and initialized to $\mathbf{F} = 1$ since the wear is completely modeled with the control inputs. The second part of the equation are the control inputs. The control input matrix $\mathbf{B}$ holds the weights calculated from the equations in Section 3.1. The control inputs vector $\mathbf{u}_k$ contains the steel grade and possible maintenance actions. The scalar $\mathbf{u}_k$ is adjusted at each heat according to the produced steel grade. Maintenance actions are updated too.

$$\begin{aligned} \mathbf{x}_{k+1} &= \underbrace{\begin{bmatrix}1\end{bmatrix}}_{\mathbf{F}} \mathbf{x}_k + \underbrace{\begin{bmatrix}w_1 & w_2 & \cdots & w_{n+1}\end{bmatrix}}_{\mathbf{B}} \underbrace{\begin{bmatrix}SG_1 \\ SG_2 \\ \vdots \\ SG_n \\ GC\end{bmatrix}}_{\mathbf{u}_k} \\ \mathbf{P}_{k+1} &= \mathbf{F}\mathbf{P}_k\mathbf{F}^T + \mathbf{Q} \end{aligned} \tag{3.2}$$

$$\begin{aligned} \mathbf{S} &= \mathbf{H}\mathbf{P}_{k+1}\mathbf{H}^T + \mathbf{R} \\ \mathbf{K} &= \mathbf{P}_{k+1}\mathbf{H}^T\mathbf{S}^{-1} \\ \mathbf{y} &= \mathbf{z} - \mathbf{H}\mathbf{x}_{k+1} \\ \mathbf{x} &= \mathbf{x}_{k+1} + \mathbf{K}\mathbf{y} \\ \mathbf{P}_{k+1} &= (\mathbf{I} - \mathbf{K}\mathbf{H})\mathbf{P}_{k+1} \end{aligned} \tag{3.3}$$

Calculating the update is only possible at points in time where laser measurements are available. Since we model the wear process with the control input matrix, we can only adjust the remaining brick depth scalar $\mathbf{x}$ with the update step. In principle, one can say this is an improved linear model with some brick depth adjustment. The scalar $\mathbf{z}$ describes a measurement value, in this case the remaining refractory brick depth obtained from a laser measurement. $\mathbf{H}$ transforms a predicted scalar $\mathbf{x}$ into a measurement to calculate the residual $\mathbf{y}$. Since $\mathbf{x}$ already holds a measurement value, the measurement matrix, which in this case is a scalar, can be set to $\mathbf{H} = 1$. $\mathbf{P}$ describes the covariance matrix and needs to be initialized at the beginning. $\mathbf{R}$ and $\mathbf{Q}$ describe the noise of the measurements and the process uncertainty.

3.2.2 Implementation

Python already provides a package for Kalman filter calculations, called FilterPy. Listing 2 shows a heavily stripped down code snippet of Model One which makes use of the FilterPy package. This should give a basic understanding how the implementation of Model One works.

```
1  from filterpy.kalman import KalmanFilter
2  import numpy as np
3
4  class KalmanModelOne(KalmanFilter):
5
6    def set_all(self, f, h, b, r, q, p):
7      self.R = r
8      self.Q = q
9      self.P = p
10     self.F = f
11     self.H = h
12     self.B = b
13     self.lastP = self.P
14
15 myKal = KalmanModelOne(dim_x= 1, dim_z = 1, dim_u=i_nr_steelgrades)
16 myKal.set_all(f=[[1.0]], h=np.array(1.0), b=B, r=100, q=1, p=20)
17
18 for heat in campaign:
19         u_k = myKal.makeSteelgradeList(heat)
20         myKal.predict(u_k)
21
22         if heat.hasLaserMeasurment:
23                 myKal.update(heat.laserMeasurment)
```

Listing 2: Excerpt of the implementation for Model One.

3.3 Kalman Filter - Model Two

3.3.1 Approach

The second model that was designed to estimate the remaining useful life of an electric arc furnace refractory brick lining is a two dimensional Kalman filter with a modified control input matrix. The prediction and update equations for this model are listed in Equation 3.4 and 3.5, respectively. The first line of the two-dimensional Kalman filter equation system implements the change of the remaining refractory brick depth while the second line of the equations accounts for the delta wear change. Since the measurements in time are sparsely distributed and the delta wear between different steel grades changes, we try to address this phenomenon with the help of modified control inputs. These control inputs calculate the gradient change of the wear that happens if the produced steel grades change. This change is fed into the model with the help of the control input vectors $\mathbf{u}_k$ and $\mathbf{u}_{k-1}$ to adjust the delta wear value. In the case when the steel grades do not change, the input controls stay zero. The adaption of the wear change Δx_k is still possible due to the Kalman filter updates. The state transition matrix is set to $\mathbf{F} = \begin{bmatrix} 1 & 1 \\ 0 & 1 \end{bmatrix}$ to account for the wear. The update equations listed in Equation 3.5 remain mostly the same. In contrast to Model One, the equation system is two dimensional. This implies that the measurement matrix $\mathbf{H}$ needs to be chosen such that it transforms the predicted vector $\mathbf{x}$ into a measurement to calculate the residual $\mathbf{y}$. This leads to a measurement matrix in the form of $\mathbf{H} = [1\ 0]$.

$$\underbrace{\begin{bmatrix} x_{k+1} \\ \Delta x_{k+1} \end{bmatrix}}_{\mathbf{x_{k+1}}} = \underbrace{\begin{bmatrix} 1 & 1 \\ 0 & 1 \end{bmatrix}}_{\mathbf{F}} \underbrace{\begin{bmatrix} x_k \\ \Delta x_k \end{bmatrix}}_{\mathbf{x_k}} + \underbrace{\begin{bmatrix} 0 & 0 & \cdots & 0 \\ w_1 & w_2 & \cdots & w_{n+1} \end{bmatrix}}_{\mathbf{B}} \left(\underbrace{\begin{bmatrix} SG_1 \\ SG_2 \\ \vdots \\ SG_n \\ GC \end{bmatrix}}_{\mathbf{u_k}} - \underbrace{\begin{bmatrix} SG_1 \\ SG_2 \\ \vdots \\ SG_n \\ GC \end{bmatrix}}_{\mathbf{u_{k-1}}} \right) \tag{3.4}$$

$$\mathbf{P}_{k+1} = \mathbf{F}\mathbf{P}_k\mathbf{F}^T + \mathbf{Q}$$

$$\begin{aligned} \mathbf{S} &= \mathbf{H}\mathbf{P}_{k+1}\mathbf{H}^T + \mathbf{R} \\ \mathbf{K} &= \mathbf{P}_{k+1}\mathbf{H}^T\mathbf{S}^{-1} \\ \mathbf{y} &= \mathbf{z} - \mathbf{H}\mathbf{x}_{k+1} \\ \mathbf{x} &= \mathbf{x}_{k+1} + \mathbf{K}\mathbf{y} \\ \mathbf{P}_{k+1} &= (\mathbf{I} - \mathbf{K}\mathbf{H})\mathbf{P}_{k+1} \end{aligned} \tag{3.5}$$

3.3.2 Implementation

As already mentioned in Section 3.2.2, FilterPy provides an implementation of the Kalman filter. For this model, we need to adjust the code to realize the modified control input calculation from Equation 3.5. Since FilterPy is implemented object oriented, it takes little effort to modify the equations. We can inherit from the KalmanFilter class and override the predict function as needed. The modified Kalman filter implementation is shown in Listing 3 as well as the update and prediction loop in pseudo code.

```
from filterpy.kalman import KalmanFilter
import numpy as np

class KalmanModelTwo(KalmanFilter):
  def predict(self, u1=0, u2=0):
      """
      Override predict function from kalman filter
      Predict next position using the Kalman filter state propagation
      equations.
      **Parameters**
      u : np.array
          Optional control vector. If non-zero, it is multiplied by B
          to create the control input into the system.
      """

      self._x = np.dot(self._F, self.x) + np.dot(self._B, u2)
          - np.dot(self._B, u1)
      self._P = self._alpha_sq * dot3(self._F, self._P, self._F.T)
          + self._Q

myKal = KalmanModelTwo(dim_x= 1, dim_z = 1, dim_u=i_nr_steelgrades)
myKal.set_all(f=[[1.0]], h=np.array(1.0), b=B, r=100, q=1, p=20)

u_k_old = myKal.makeSteelgradeList(heat)
for heat in campaign:
        u_k = myKal.makeSteelgradeList(heat)
        myKal.predict(u_k_old, u_k)
        u_k_old = u_k

        if heat.hasLaserMeasurment:
                myKal.update(heat.laserMeasurment)
```

Listing 3: Excerpt of the implementation for Model Two.

3.4 Kalman Filter - Model Three

3.4.1 Approach

The third model that was designed to estimate the remaining brick depth of an electric arc furnace is a multidimensional Kalman filter without control inputs. Since we know that different steel grades lead to different wear, we try to model the gradient of each steel grade with an explicit wear delta. An additional delta for the maintenance actions is introduced. The equations for the prediction and update step are listed in Equation 3.6 and Equation 3.7. The state transition matrix $\mathbf{F}$ is a square matrix. It's size is determined by the number of steel grades plus one. The matrix is initialized with zeros and its main diagonal is set to one. At each heat, the entries of the first row are modified according to the produced steel grade and the performed maintenance actions. The first entry of vector $\mathbf{x}$ is initialized to the brick depth and the other entries are initialized to the calculated average delta wear values from the least squares calculations. The measurement matrix $\mathbf{H}$ is initialized as a one-dimensional vector with zeros, but its first entry is set to one. This is needed to calculate the residual $\mathbf{y}$ of the real laser measurement and the predicted measurement.

$$\underbrace{\begin{bmatrix} x[k+1] \\ \Delta x_1[k+1] \\ \Delta x_2[k+1] \\ \vdots \\ \Delta x_{n+1}[k+1] \end{bmatrix}}_{\mathbf{x}_{k+1}} = \mathbf{F} \underbrace{\begin{bmatrix} x[k] \\ \Delta x_1[k] \\ \Delta x_2[k] \\ \vdots \\ \Delta x_{n+1}[k] \end{bmatrix}}_{\mathbf{x}_k} \tag{3.6}$$

$$\mathbf{P}_{k+1} = \mathbf{F}\mathbf{P}_k\mathbf{F}^T + \mathbf{Q}$$

$$\begin{aligned} \mathbf{S} &= \mathbf{H}\mathbf{P}_{k+1}\mathbf{H}^T + \mathbf{R} \\ \mathbf{K} &= \mathbf{P}_{k+1}\mathbf{H}^T\mathbf{S}^{-1} \\ \mathbf{y} &= \mathbf{z} - \mathbf{H}\mathbf{x}_{k+1} \\ \mathbf{x} &= \mathbf{x}_{k+1} + \mathbf{K}\mathbf{y} \\ \mathbf{P}_{k+1} &= (\mathbf{I} - \mathbf{K}\mathbf{H})\mathbf{P}_{k+1} \end{aligned} \tag{3.7}$$

3.4.2 Implementation

We again use FilterPy for the implementation of Model Three. No modifications are needed and we just have to design our matrices accordingly. Listing 4 shows the pseudo code for the implementation. As one can see, in contrast to the other two models, this implementation does not have any arguments in the predict function since this is the only model without control inputs.

```
from filterpy.kalman import KalmanFilter
import numpy as np

class KalmanModelThree(KalmanFilter):

  def set_all(self, f, h, b, r, q, p):
    self.R = r
    self.Q = q
    self.P = p
    self.F = f
    self.H = h
    self.B = b
    self.lastP = self.P

myKal = KalmanModelThree(dim_x= 1, dim_z = 1, dim_u=i_nr_steelgrades)
myKal.set_all(f=[[1.0]], h=np.array(1.0), b=B, r=100, q=1, p=20)

for heat in campaign:
        myKal.predict()

        if heat.hasLaserMeasurment:
                myKal.update(heat.laserMeasurment)
```

Listing 4: Excerpt of the implementation for Model Three.

4 Evaluation

Contents

4.1 Least Squares Evaluation 33
4.2 Model One Evaluation 35
4.3 Model Two Evaluation 39
4.4 Model Three Evaluation 42
4.5 Comparison 45
4.6 Insights on Q and R 47
4.7 Quality of Laser Measurments 50

In this chapter we discuss the results of the different models and also take a closer look at the laser measurements of the different campaigns. Out of 52 provided campaigns, only the last 22 contain valid maintenance data. Therefore we will focus on these 22 campaigns for our evaluation.

4.1 Least Squares Evaluation

As described in Section 3.1 we solve an overdetermined system of equations with least squares. For these calculations, only campaigns have been used that contain valid maintenance information. Campaigns that contain obviously wrong data are disregarded. For all steel grades that have been produced more than 400 times over these 22 campaigns, a separate delta wear is calculated. Steel grades that have been produced less than this threshold are consolidated in a general steel grade called “Other”. Figure 4.1 shows the result of these calculations.

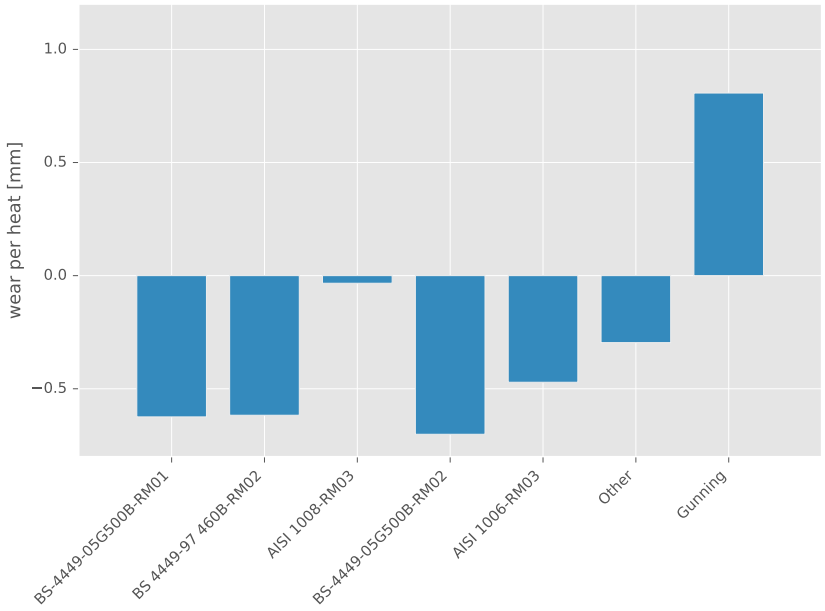

Figure 4.1: Estimated average wear per heat for Hot Spot 1 for steel grades produced more than 400 times.

From Figure 4.1 it can be seen that from the 29 different steel grades produced only five occur more than 400 times over the given data set. All the other steel grades are combined in the penultimate bar labeled "Other". The last bar shows the impact of the gunning maintenance per heat. One can say that most of the steel grades cause an average wear around 0.6mm per heat except of steel grade "AISI 1008-RM03", which causes a significant lower wear. However, it is crucial to point out that the laser data is very noisy. We assume that the real wear is probably higher since we don't know how the gunning material behaves exactly. RHI experts suspect that the refractory maintenance material wears out much faster than the refractory bricks. Furthermore, in reality the gunning mass would have a much higher impact than calculated. The laser measurements are way too sparse to account for these assumptions. However, these calculations build the basis for our three models.

4.2 Model One Evaluation

The control input matrix $\mathbf{B}$ of our first model is initialized with the steel grade and gunning weights calculated from the least squares method described in Section 4.1. For each campaign to be tested with the model the specific campaign from the least squares calculations is excluded. This approach is known as "Leave-one-out cross validation". The control input vector $\mathbf{u}_k$ is changed according to the produced steel grade and gunning action performed. The measurement noise matrix is initialized to $\mathbf{R} = 100$ and the process noise matrix is set to $\mathbf{Q} = 0.1$. The covariance matrix is initialized with $\mathbf{P} = 10000$.

Figure 4.2 shows the estimated prediction of this first model. The thick blue line indicates the ground truth. The ground truth is calculated from the mean of the remaining brick depth in Hot Spot 1. The darker blue shaded area indicates one standard deviation of Hot Spot 1 and the lighter blue shaded area indicates twice the standard deviation of the Hot Spot 1 laser measurements. The different colors in the background indicate different steel grades. The dashed green lines visualize at which heats laser measurements were taken and the blue bar plots depict the consumed refractory material in kg used by gunning for this area. Each of the colored lines indicates one prediction. The first prediction starts at the first laser measurement named "LM 1". Therefore, the model receives no further updates. The second prediction line starts at the second laser measurement. Obviously, the second prediction receives a model update at laser measurement one but no updates are performed after "LM 1". This concept is continued for the remaining prediction lines. To make this more clear, Figures 4.3 - 4.5 show this concept up to the first three predictions. Figure 4.3 depicts the first prediction line. Figure 4.4 shows the first and second prediction lines where the second prediction received an update at the first laser measurement and the third prediction received an update at laser measurement one and laser measurement two.

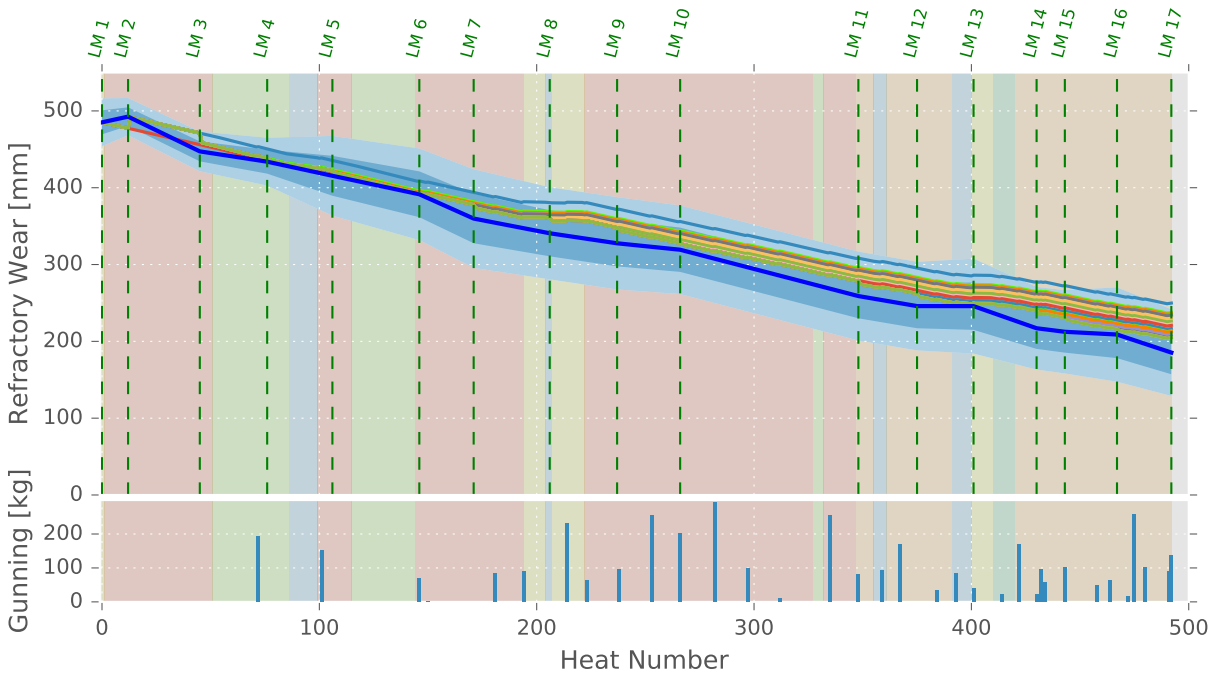

Figure 4.2: Campaign 40; The blue line indicates the mean of the remaining brick depth in Hot Spot 1 and the blue shaded areas indicate one standard deviation and two times the standard deviation. The colored lines are the prediction of Model One. The first prediction starts at laser measurement one and the model isn't updated after that. The second prediction starts at laser measurement two, etc. The different colors in the background indicate different produced steel grades. The vertical green dashed lines depict the heats where laser measurements were taken. The blue bars show the gunning consumption in kg.

As one can see, the more laser measurement updates the model receives, the better the prediction gets, evaluated on the last measurement in time. We are not interested in calculating an error measure over the whole campaign, since faulty measurements, outliers and wrong positioning of the laser influences the result. For APO it is essential to know how many heats the EAF lasts and therefore we are interested in how many heats are possible until a critical brick depth is reached. Since most campaigns end before the critical brick depth is reached, we have to evaluate our models on the last measurement of each campaign. Therefore, we calculate the root mean squared error (RMSE) between the last prediction value and the last measurement. These calculations are shown in Figure 4.6. Figure 4.6 confirms our visual observations from Figure 4.2 that the predictions get better over time.

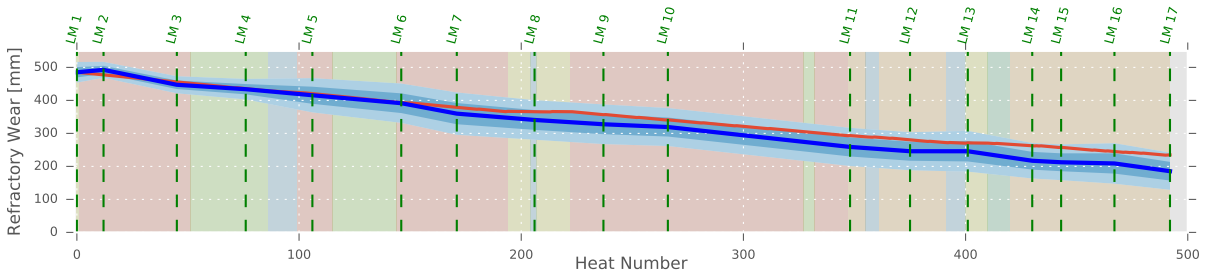

Figure 4.3: Prediction, starting from the first laser measurement.

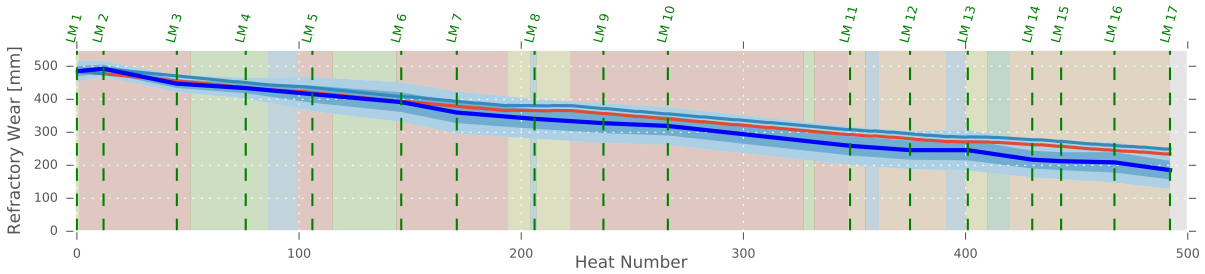

Figure 4.4: Second prediction, starting from the second laser measurement.

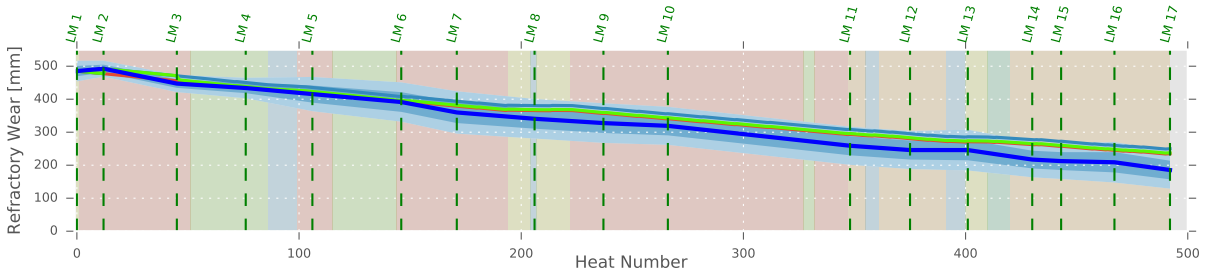

Figure 4.5: Third prediction, starting from the third laser measurement.

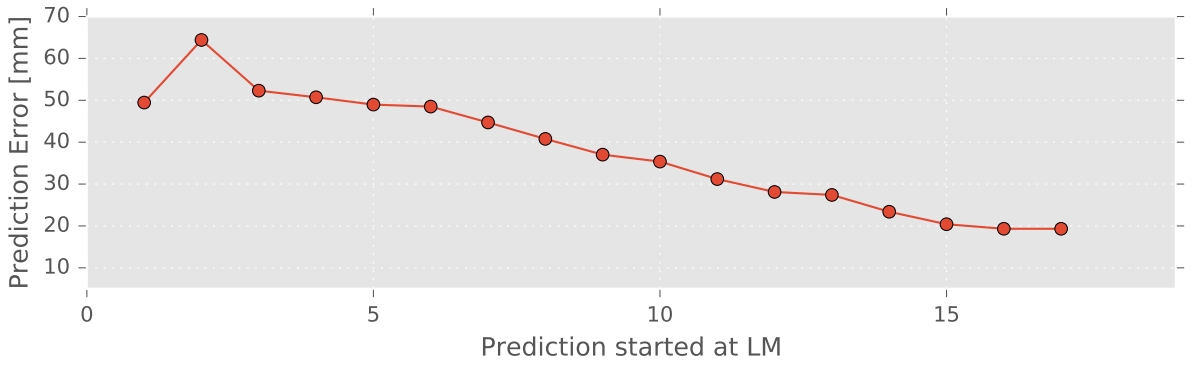

Figure 4.6: RMSE over all predictions started at different laser measurements evaluated at the end of the campaign.

Figure 4.7 shows the RMSE with its standard deviation over a selection of 18 tested campaigns since four campaigns contain obviously false measurements which would lead to a worse RMSE.

Since each campaign consists of a different amount of heats, we divided each campaign in eight equal parts. All predictions that start in the same part are collected over all campaigns to calculate a mean error and its corresponding standard deviation. One can observe from Figure 4.7 that on average Model One has a solid prediction accuracy from the beginning on and the accuracy is getting better over the duration of the campaigns.

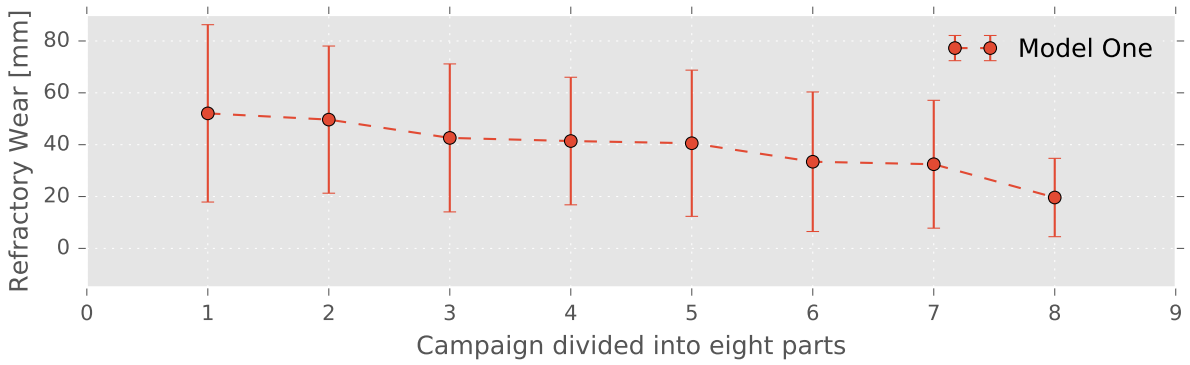

Figure 4.7: RMSE over all campaigns. Each campaign is divided into eight equal parts.

4.3 Model Two Evaluation

For Model Two we initialize the input control matrix $\mathbf{B}$ with the weights calculated from least squares like we did for Model One. In contrast to Model One, this time we calculate the difference of the delta wear of two consecutive heats in the control inputs. As long as the produced steel grade does not change and there is also no change in the maintenance actions applied, the difference equals to zero and therefore the control inputs do not contribute to the model. The vector $\mathbf{u}_k$ again holds the produced steel grade and also maintenance actions that happened. Additionally, a second control input vector $\mathbf{u}_{k-1}$ is needed that holds the produced steel grade and maintenance actions of the previous heat.

In Figure 4.8 the estimated wear of Hot Spot 1 for campaign 40 calculated from Model Two is shown. Again, the darker shaded blue areas indicate one standard deviation of Hot Spot 1 while the lighter area indicates twice the standard deviation. The colored lines show the predictions starting at different laser measurements while the thicker blue line depicts the ground truth calculated from the mean of Hot Spot 1. In contrast to the first model, Model Two does not only update the remaining brick depth values but updates a general wear value Δx, too. Figure 4.9 shows this change of Δx over the whole campaign. The spikes indicate that maintenance in terms of gunning happened. The control inputs also cause changes when the produced steel grades change. The changes that are caused from the correction step of the Kalman filter can be observed at the time steps where a laser measurement happened, since these are the only points in time the Kalman filter receives values to update the model. Laser measurements were taken at each green dashed line. One can clearly see how the modified input controls of this model change the delta wear value at each steel grade change. Different values for $\mathbf{R}$ and $\mathbf{Q}$ lead to different magnitudes of correction of Δx. The laser measurement updates adapt the general wear Δx only by small amounts because the second entry of the main diagonal of the process noise matrix is set to very small values, i.e. $\mathbf{Q} = 0.0001$. This is done to prevent the model to correct itself based on false measurements or manually performed maintenance that is not reflected in the data set. The measurement noise matrix is set to $\mathbf{R} = 500$ and the covariance matrix is initialized by $\mathbf{P} = 10000$. If we would increase $\mathbf{Q}$ to bigger values, we would get significant updates at the laser measurements. This updates cause large changes in the gradient Δx and effect the model negatively. Further information on the process noise matrix and the measurement noise matrix are discussed in Section 4.6
Figure 4.10 shows the prediction error of campaign number 40. The error is calculated analogously to Model One. The observations from Model One hold true for Model Two. The predictions are getting better towards the end of the campaign.

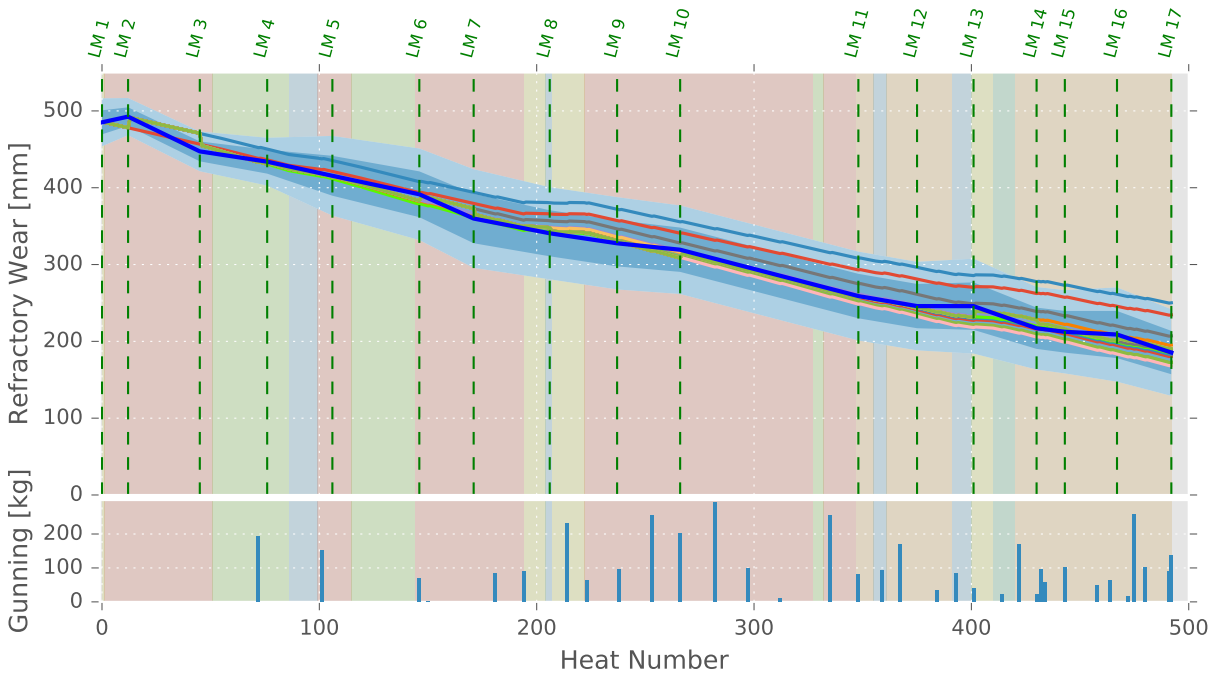

Figure 4.8: Campaign 40; The blue line indicates the mean of the remaining brick depth in Hot Spot 1 and the shaded blue areas indicate one standard deviation and two times the standard deviation. The colored lines are the prediction of Model Two. The first prediction starts at laser measurement one and the model isn't updated after that. The second prediction starts at laser measurement two, etc. The different colors in the background indicate different produced steel grades. The vertical green dashed lines depict the heats where laser measurements were taken. The blue bars show the gunning consumption in kg.

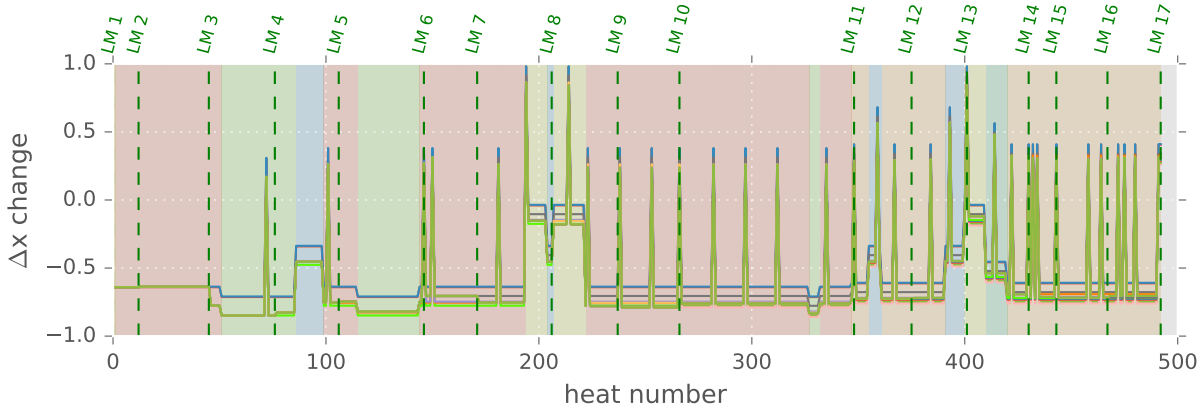

Figure 4.9: Change of Δx over the course of the campaign. Each line represents one prediction.

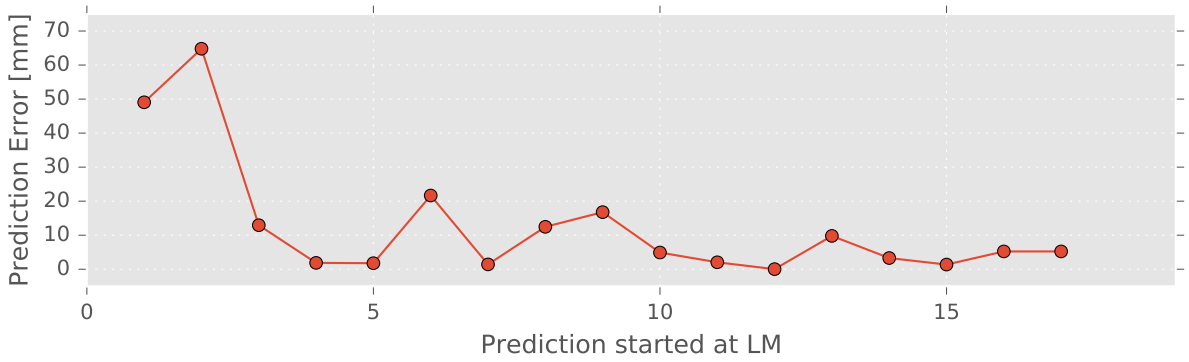

Figure 4.10: RMSE over all predictions started at different laser measurements evaluated at the end of the campaign.

Figure 4.11 shows the prediction error over the previously tested 18 campaigns. As in the evaluation of Model One we again divided all campaigns into eight equal parts. For each prediction started in one part the mean error and its standard deviation are calculated. One can observe from the plot that on average the prediction is getting better in the second half of a campaign.

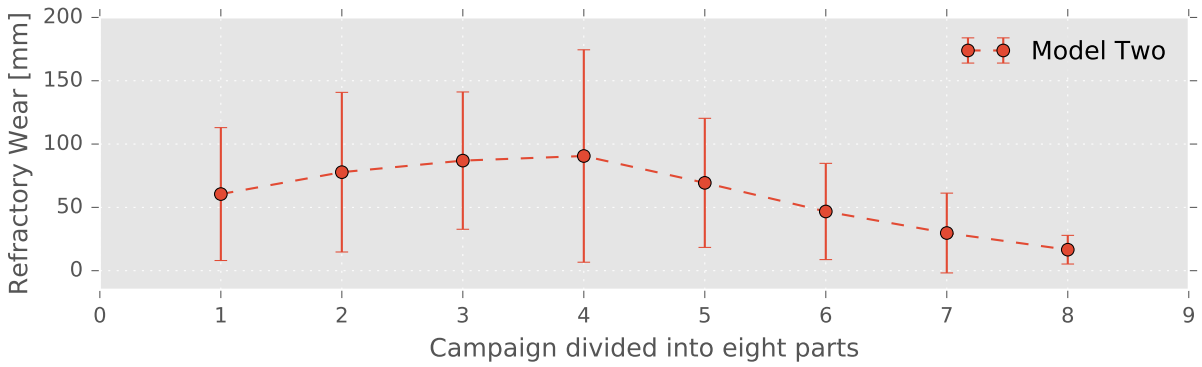

Figure 4.11: RMSE over all campaigns. Each campaign is divided into eight equal parts.

4.4 Model Three Evaluation

Model Three is designed to adapt itself completely. No additional control inputs are needed. The state vector $\mathbf{x}$ of Model Three is initialized with the delta wear learned from least squares. As mentioned before, Model Three does not have a control input matrix. Each steel grade that occurs more than 400 times over the campaigns is modeled with a separate delta wear parameter in the vector $\mathbf{x}$. Additionally, a parameter for maintenance actions in the form of gunning is added to the state vector $\mathbf{x}$. The first row of the state transition matrix $\mathbf{F}$ is adapted to the according production plan parameters. We set the measurement noise matrix $\mathbf{R} = 500$ and the main diagonal of the process noise matrix $\mathbf{Q} = 0.00015$ except the first entry of $\mathbf{Q}[0,0] = 5.0$. The main diagonal of the covariance matrix $\mathbf{P}$ is initialized to $\mathbf{P} = 0.25$ and its first entry to $\mathbf{P}[0,0] = 10000$. Figure 4.12 shows the prediction of this model. At first sight, there is not much difference to the previous two models. If we take a closer look at the delta wear values for the different steel grades, we can see that Model Three adapts to the different produced steel grades. Figure 4.13 depicts this change of the delta wear value. Each line in Figure 4.13 represents one steel grade from the vector $\mathbf{x}$ for the prediction with updates until the last laser measurement.

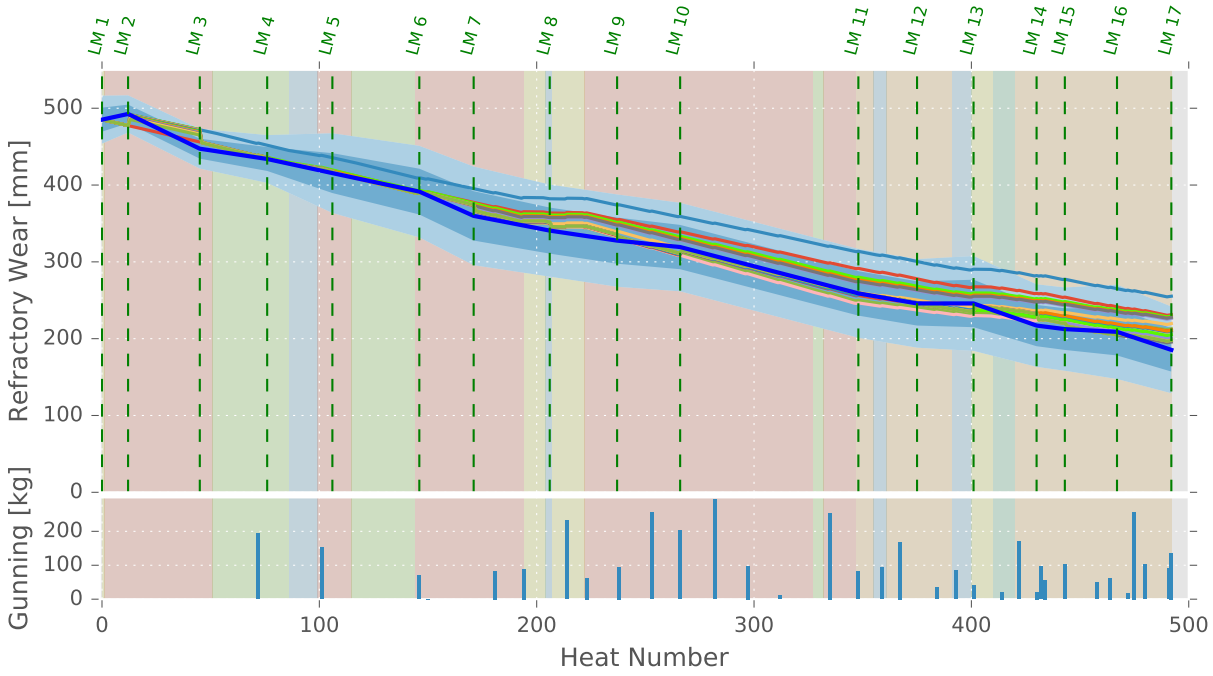

Figure 4.12: Campaign 40; The blue line indicates the mean of the remaining brick depth in Hot Spot 1 and the shaded blue areas indicate one standard deviation and two times the standard deviation. The colored lines are the prediction of Model Three. The first prediction starts at laser measurement one and the model isn't updated after that. The second prediction starts at laser measurement two, etc. The different colors in the background indicate different produced steel grades. The vertical green dashed lines depict the heats where laser measurements were taken. The blue bars show the gunning consumption in kg.

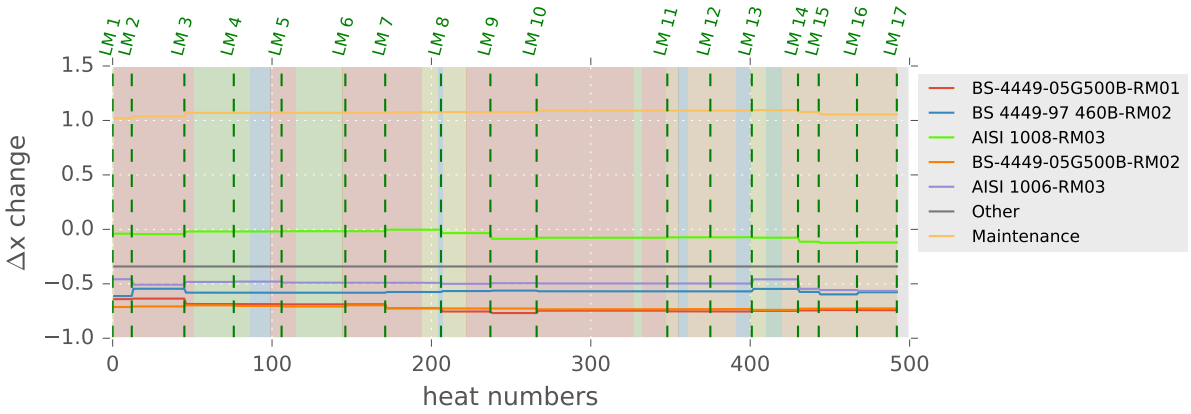

Figure 4.13: Change of Δx over the course of the campaign. Each line represents one entry of the state vector $\mathbf{x}$ except the first entry, namely brick depth itself.

Figure 4.14 shows the prediction error of campaign nr. 40. The error is calculated analogously to Model One and Model Two. Again the observations from Model One hold true for Model Two. The predictions are getting better towards the end of the campaign.

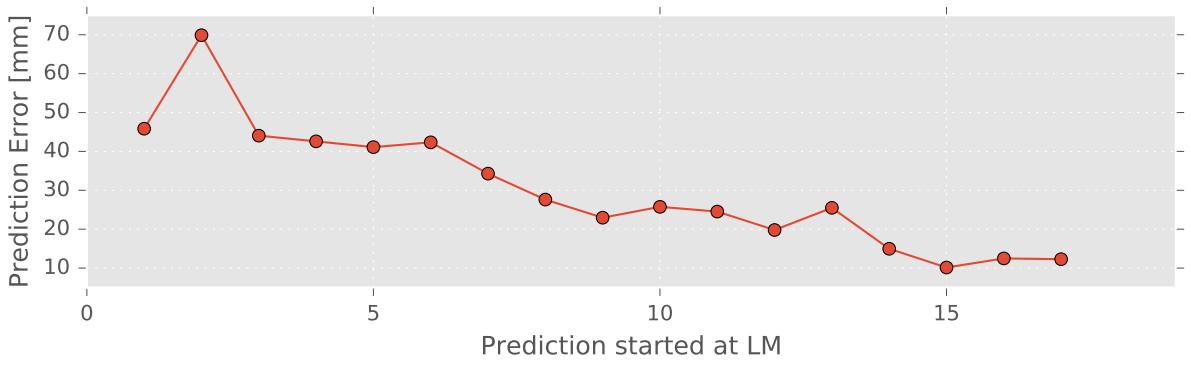

Figure 4.14: RMSE for all predictions started at different laser measurements evaluated at the end of the campaign.

Identical to the other models, we divided each campaign into eight different parts. For each of these parts the mean error of all predictions starting in this part are calculated over all 18 campaigns. These calculations are shown in Figure 4.15.

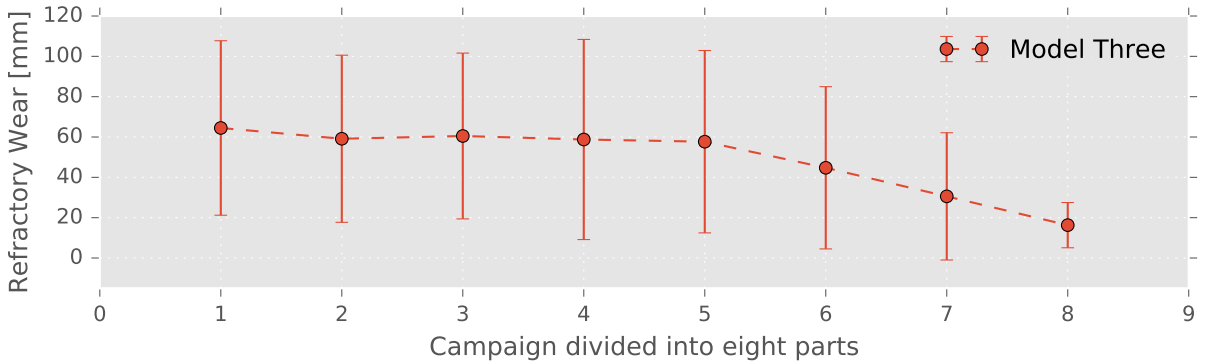

Figure 4.15: RMSE over all campaigns. Each campaign is divided into eight equal parts.

4.5 Comparison

In this section the errors of all three models are compared. First, we will take a look at the previously shown campaign number 40. Figure 4.16 shows the mean error of all three models for this campaign. As one can see, Model Two performs best for campaign number 40. This observation is specific to this campaign and is not representative over all tested campaigns. Figure 4.17 depicts the mean prediction error over all campaigns of all three models. All campaigns are divided into eight equal parts. All predictions that start in a specific part are collected over the whole range of campaigns and the mean error and the standard deviation are calculated. One can see from this plot that on average Model One and Model Three provide the best predictions. Model One performs slightly better in the first half of the campaigns. Towards the end of the campaigns, Model Three provides slightly better predictions with smaller errors than the other two models. It is important to state that these observations hold true as long as the used refractory bricks and maintenance material don't change significantly. If maintenance material is used that has a better durability, Model One would probably lead to worse predictions than the other two models, since Model One heavily relies on the calculations from least squares and is not able to adapt the wear rates.

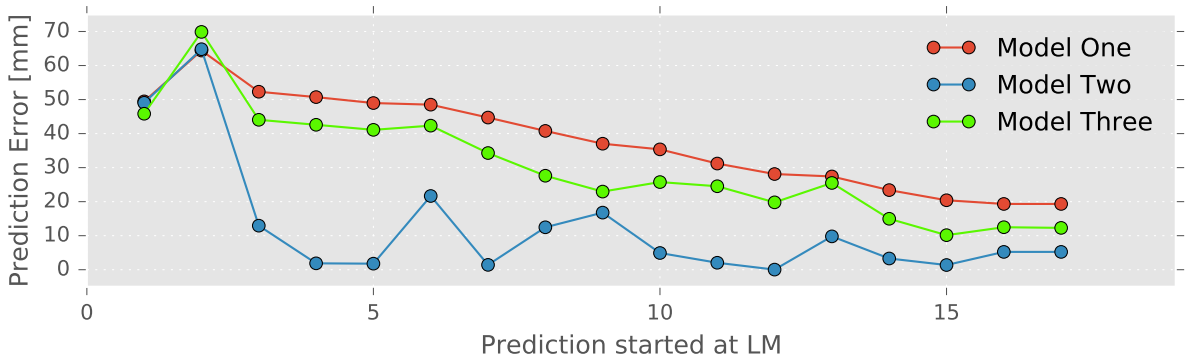

Figure 4.16: Comparison of RMSE for all three models on campaign Nr. 40.

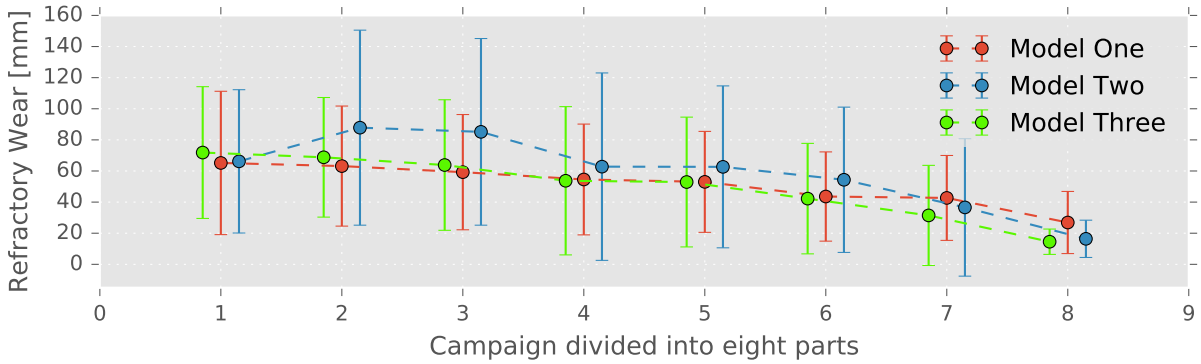

Figure 4.17: Comparison of RMSE with standard deviation over all campaigns for all three models.

To gather more detailed insights, Table 4.1 shows the mean error for each campaign and each model separately. The highlighted green cells indicate the lowest error for each part of the

campaigns over the three models. Empty cells indicate that no laser measurements took place in a given part of the campaign.

Campaign 30	Model 1		62.44	59.43	57.48	59.14	54.71	46.94	42.31
	Model 2		61.25	68.20	53.04	61.20	33.80	20.77	13.09
	Model 3		63.06	59.31	55.63	60.14	39.90	24.58	15.77
Campaign 31	Model 1	3.31	30.84	27.64	17.62	12.04	17.26		14.83
	Model 2	2.71	132.16	39.03	29.44	16.69	30.20		12.06
	Model 3	14.27	37.06	23.95	5.74	2.52	34.83		13.85
Campaign 32	Model 1	15.62	19.91	20.35	24.67	25.90	23.50	9.31	6.29
	Model 2	14.97	18.26	35.28	49.71	44.69	35.26	27.63	11.67
	Model 3	26.71	32.52	35.63	44.16	42.86	30.94	13.89	11.99
Campaign 33	Model 1	14.13	7.94	1.78	0.91	9.81	14.63	14.33	14.50
	Model 2	15.70	70.43	47.88	22.01	32.34	29.05	17.31	15.47
	Model 3	23.60	7.68	4.53	2.51	23.36	17.51	9.67	12.34
Campaign 34	Model 1	41.72	43.28	48.42	51.58	52.37	44.74	40.69	33.49
	Model 2	41.21	58.27	88.80	78.34	60.43	17.67	23.07	14.33
	Model 3	57.13	62.14	68.11	71.17	52.96	10.00	20.46	13.11
Campaign 35	Model 1	121.23	110.06	102.12	79.08	65.57	55.02	50.92	50.92
	Model 2	121.88	98.85	60.56	30.27	9.00	5.28	8.15	8.15
	Model 3	111.24	93.94	86.81	21.35	15.79	7.18	15.56	15.81
Campaign 36	Model 1		39.01	25.32	22.33	45.06	67.04	81.11	62.45
	Model 2		39.40	19.64	9.42	144.60	164.38	154.82	42.39
	Model 3		44.56	23.93	17.96	60.36	83.25	102.24	21.35
Campaign 37	Model 1	56.93	51.51	48.74	42.75	37.02	35.36	28.90	21.04
	Model 2	56.92	7.41	11.72	6.94	16.78	4.91	3.96	3.30
	Model 3	57.86	43.32	41.72	30.95	22.96	25.75	23.27	12.53
Campaign 38	Model 1	170.79	160.39	155.35	141.38	115.95	101.88	89.50	84.18
	Model 2	169.21	148.98	112.33	41.57	19.48	6.40	14.32	27.31
	Model 3	159.71	143.49	136.57	115.96	61.86	44.14	21.98	44.39
Campaign 39	Model 1	87.54	54.79		39.05	16.71	3.46	3.16	5.57
	Model 2	87.53	107.68		45.24	94.83	76.20	53.11	31.16
	Model 3	83.37	36.20		25.97	37.45	47.17	40.62	23.88
Campaign 40	Model 1	85.77	78.70	78.07	75.51	68.44	56.23	46.33	29.13
	Model 2	86.13	63.79	76.61	54.56	26.40	6.82	6.82	13.19
	Model 3	87.21	73.33	72.69	65.35	49.78	21.95	15.74	7.27
Campaign 41	Model 1	67.15	72.16	76.52	94.78	100.05	91.41	74.09	50.11
	Model 2	81.32	86.33	101.87	217.86	158.35	78.87	21.63	8.98
	Model 3	90.33	99.93	106.72	195.05	178.45	107.74	37.89	12.40
Campaign 42	Model 1	22.77	37.18	58.08	60.15	63.00	47.05	13.48	5.42
	Model 2	26.07	119.95	185.38	117.99	102.27	71.48	63.79	24.24
	Model 3	35.99	64.47	88.14	90.70	94.79	49.86	14.79	9.94
Campaign 43	Model 1		44.22	26.34	32.23	25.96	29.06	24.16	14.31
	Model 2		44.52	36.06	39.74	0.99	29.74	9.87	10.04
	Model 3		45.72	15.95	23.12	12.96	21.58	5.50	17.48
Campaign 44	Model 1	34.01	55.28	69.05		79.34	90.96	95.54	
	Model 2	34.28	79.19	116.00		131.53	138.78	126.40	
	Model 3	36.51	70.74	92.64		108.80	120.69	116.33	
Campaign 45	Model 1	59.77	91.58	58.57	32.96	14.35	2.04	3.09	3.09
	Model 2	59.80	191.10	165.64	196.33	128.16	95.70	38.02	38.02
	Model 3	57.95	120.25	21.93	21.08	52.47	67.79	25.85	25.58
Campaign 46	Model 1	115.29	115.97	119.56	104.25	85.86	64.77	52.80	36.88
	Model 2	108.81	129.48	141.44	35.47	14.74	20.07	1.84	13.30
	Model 3	123.45	122.44	129.93	79.83	29.37	4.20	10.56	8.33

Table 4.1: Mean error for each campaign and model. All campaigns are divided into eight equal parts. Green cells indicate the lowest error of a given model for each part of a campaign.

4.6 Insights on Q and R

In order to discuss the influence of the measurement noise matrix $\mathbf{R}$ and the process noise matrix $\mathbf{Q}$, we select a campaign which is not as smooth as the already discussed campaign in the evaluations. We show the influence of these parameters on Model Three, but the general concept applies to all three models. The analysis is done on campaign number 51. Figure 4.18 shows the prediction with all parameters set as in the evaluation of Model Three.
Figure 4.19 shows the prediction line with all updates until the latest laser measurement. The measurement noise matrix is set to $\mathbf{R} = 100$. One can see that the Kalman filter clearly trusts the measurements and subsequently corrects the prediction of the remaining refractory lining depth to the measurement. In contrast, Figure 4.20 shows the same prediction with a measurement noise matrix set to $\mathbf{R} = 1000$. The high value of $\mathbf{R}$ tells the filter to trust the measurements less. This can be clearly observed in Figure 4.20. These observations should make our choice of the measurement matrix $\mathbf{R} = 500$ obvious, since this is a trade off between too much and too little correction.

Similar conclusions can be drawn for the process noise $\mathbf{Q}$. Setting the process noise matrix to a rather big value $\mathbf{Q} = 0.01$ leads to significant updates of the delta wear values in the state vector $\mathbf{x}$. This behavior can be observed in Figure 4.21. As one can see at the first occurrence of the steel grade, indicated with the red background color, significant updates are made for the wear of this steel grade. At the second occurrence, this wear leads to very false predictions. Figure 4.22 shows the same predictions with a smaller process noise matrix $\mathbf{Q} = 0.0001$. The updates of the state vector $\mathbf{x}$ are not as aggressive as shown in Figure 4.21.
From these insights it is obvious that the process noise and measurement noise matrices need to be designed carefully. A trade off between adaption and good prediction capabilities has to be made.

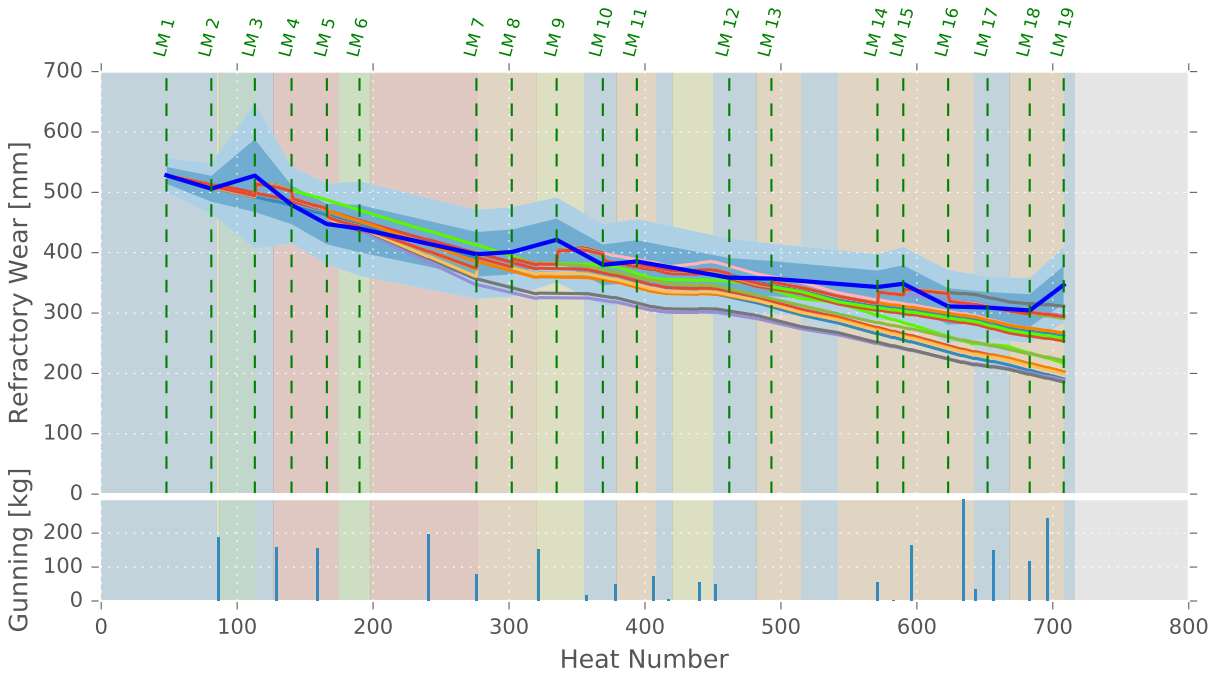

Figure 4.18: Campaign 51; Prediction with all updates on each laser measurement. Measurement noise matrix $\mathbf{R} = 500$ *and process noise matrix* $\mathbf{Q} = 0.0001$.

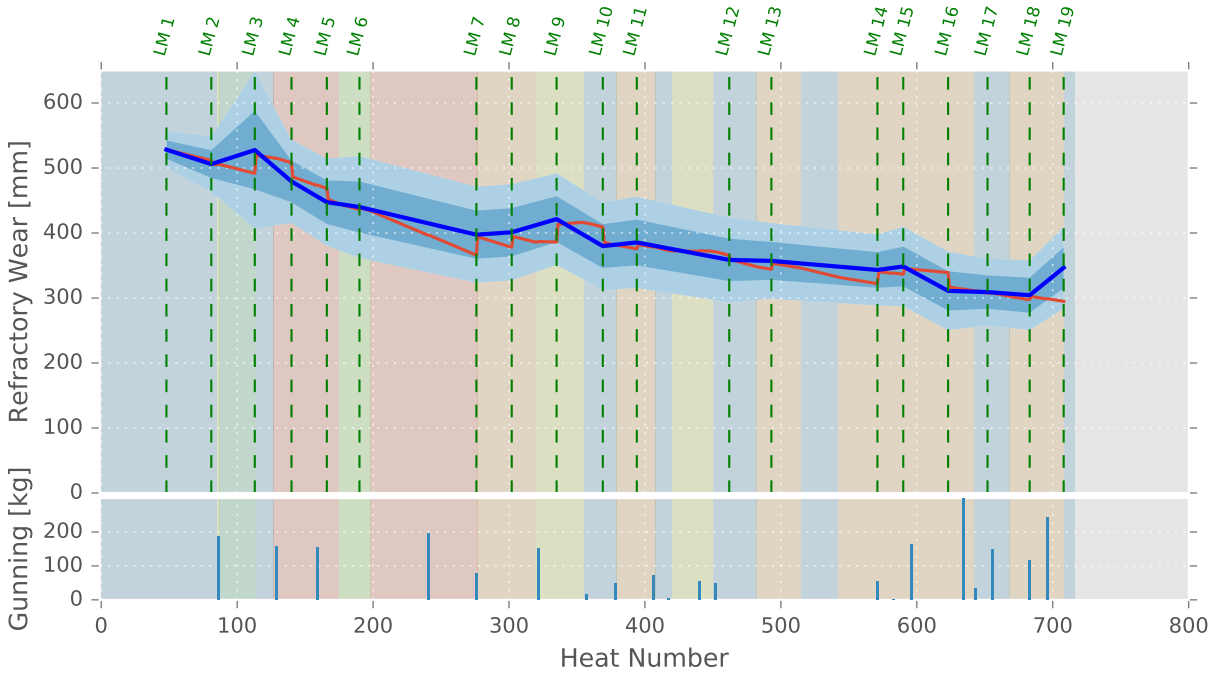

Figure 4.19: Campaign 51; Prediction with all updates on each laser measurement. Measurement noise matrix $\mathbf{R} = 100$ *and process noise matrix* $\mathbf{Q} = 0.0001$.

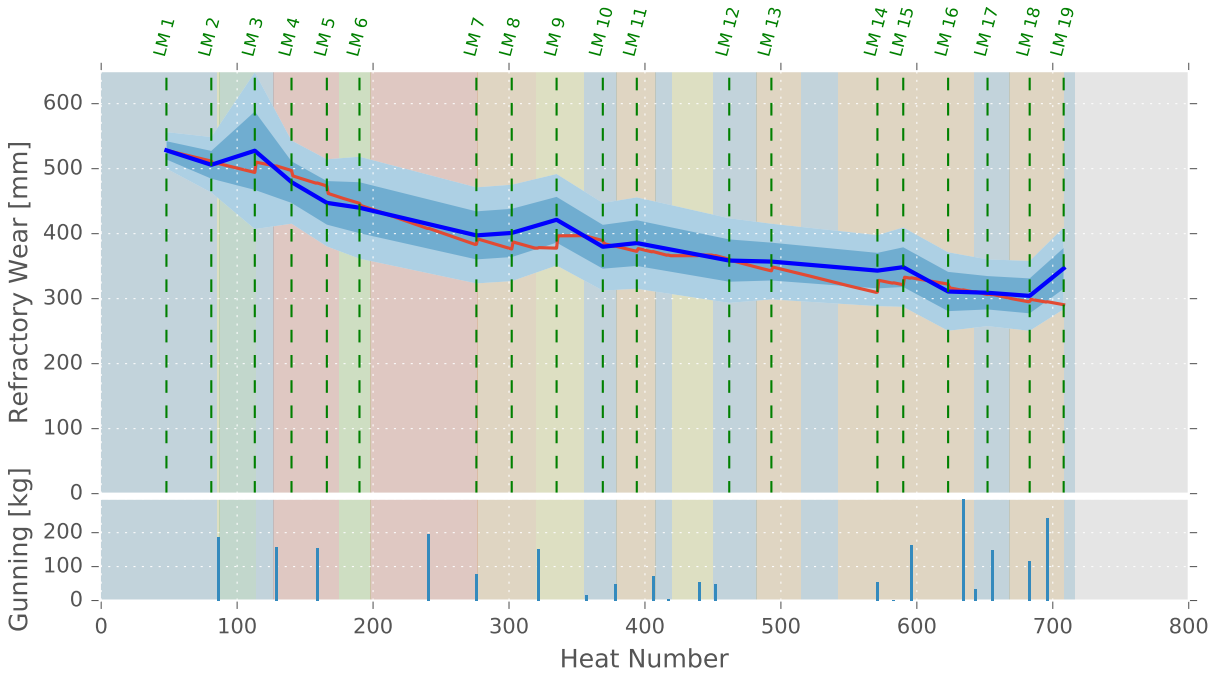

Figure 4.20: Campaign 51; Prediction with all updates on each laser measurement. Measurement noise matrix $\mathbf{R} = 1000$ *and process noise matrix* $\mathbf{Q} = 0.0001$.

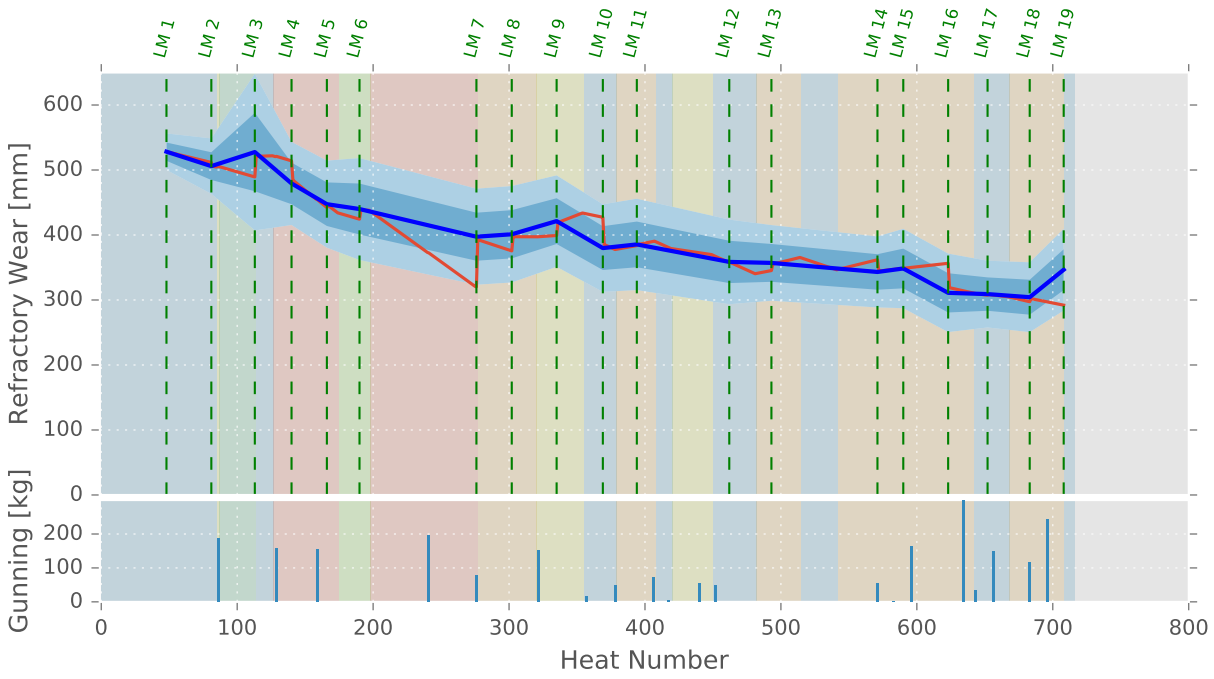

Figure 4.21: Campaign 51; Prediction with all updates on each laser measurement. Measurement noise matrix $\mathbf{R} = 500$ *and process noise matrix* $\mathbf{Q} = 0.01$.

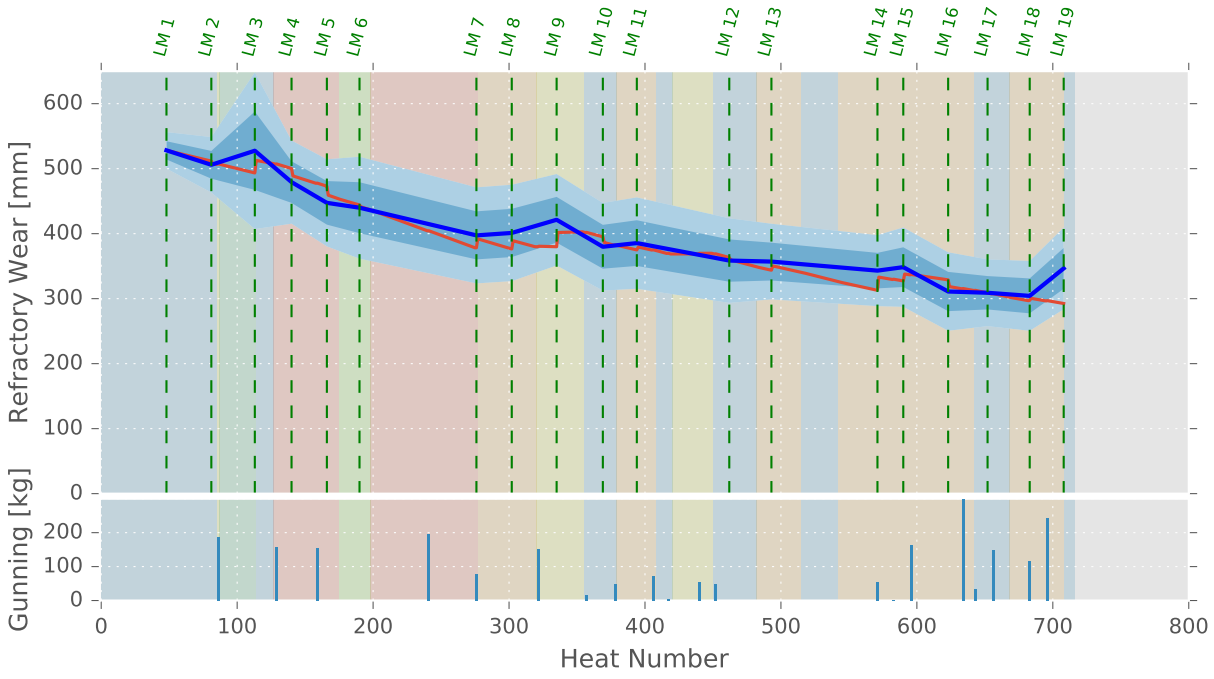

Figure 4.22: Campaign 51; Prediction with all updates on each laser measurement. Measurement noise matrix $\mathbf{R} = 500$ *and process noise matrix* $\mathbf{Q} = 0.0001$.

4.7 Quality of Laser Measurments

Several challenges exist that need to be solved. In this section we point out the things that we discovered over the course of this work. We calculated the mean and standard deviation of the laser measurements in Hot Spot 1. As described earlier, the blue shaded areas in the plot indicate one standard deviation and twice the standard deviation respectively. One can clearly see that from the Figures 4.23 - 4.25 that the laser measurements vary a lot. This could be caused because the definition of Hot Spot 1 is not optimal. Further investigation on this topic needs to be conducted.
From Figure 4.23 one can clearly see that the positioning of the laser is sometimes not optimal. This campaign is an extreme example but leads to the assumption that other campaigns are also affected, even if it is not as obvious.
In Figure 4.24 one can see several anomalies in the first half of the campaign. Around heat number 100 the refractory lining depth is suddenly thicker without maintenance action. The same happens again around heat 350. Other campaigns exist where the same phenomenon can be observed. We don't know if these increases in brick depth come from slag that remains on the refractory bricks or if it is a cause of the laser positioning issues mentioned above. Figure 4.25 depicts another issue. The cause of the sudden increase of refractory brick depth around heat 450 remains unknown to us. We found from further investigation that there was a timespan of 12 hours in which no steel has been produced. That leads to the assumption that manual maintenance has been performed. It should be considered to include annotations into the data set if such things happen.

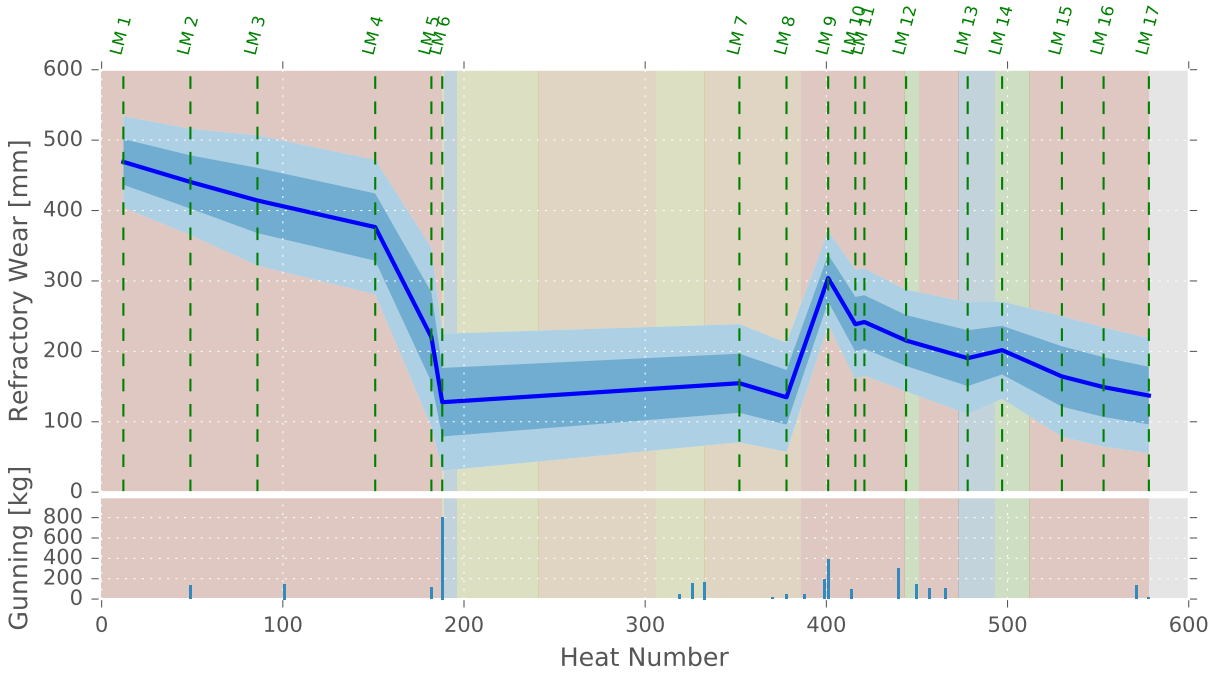

Figure 4.23: Campaign 44; Sample campaign to show laser positioning issues.

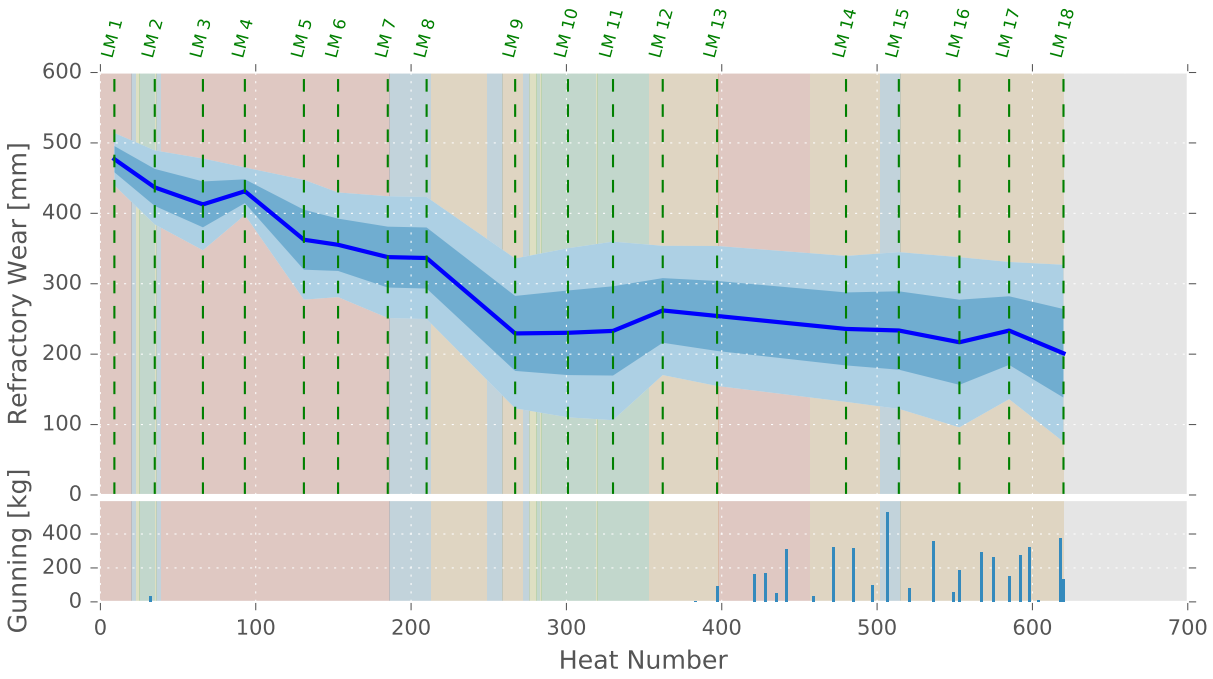

Figure 4.24: Campaign 45; Unknown increase of refractory brick depth with no obvious cause.

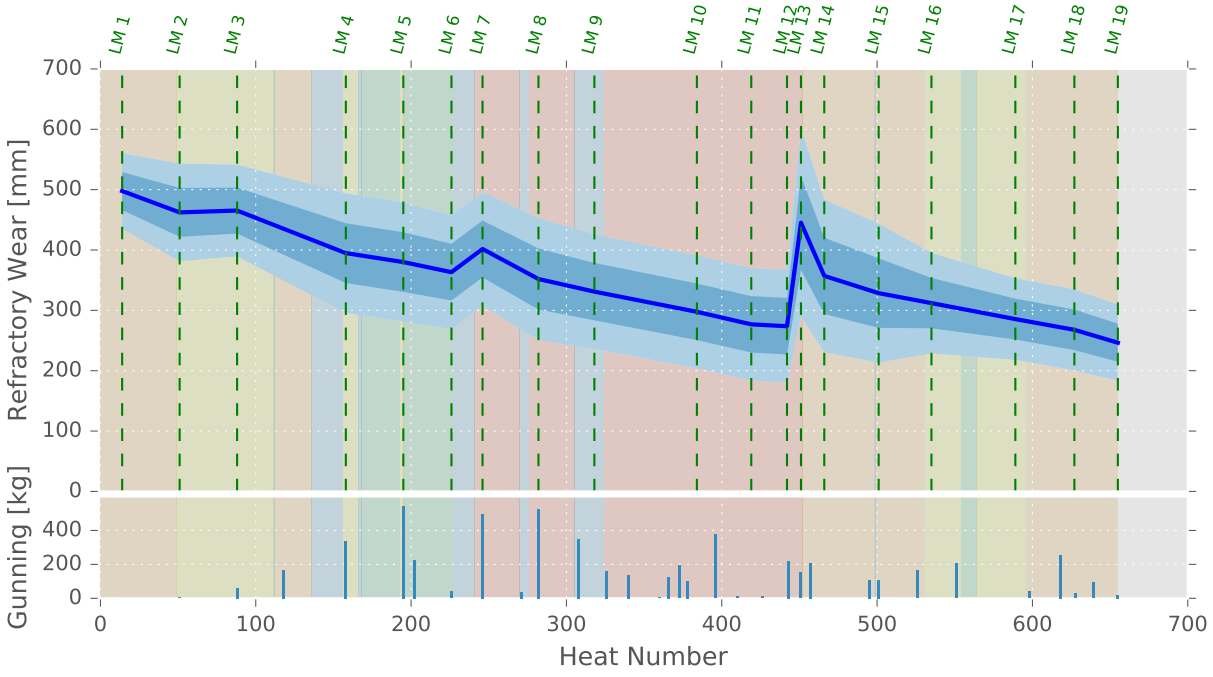

Figure 4.25: Campaign 46; Increase of refractory brick depth with 12 hour production pause.

5 Conclusion and Future Work

Contents

5.1 Conclusion 53
5.2 Future Work 54

5.1 Conclusion

This thesis shows that it is possible to predict the remaining refractory brick depth from a predefined production plan with a linear model. This production plan only contains the steel grades that are going to be produced in each heat. Furthermore, the production plan includes information about maintenance actions that take place. For this research the only maintenance action considered is gunning.
Three models have been developed and tested. The first model is a simple linear wear model which heavily relies on its initialization from the least squares solution of an overdetermined set of linear equations. The second model is an improvement over the first model in terms of its adaption abilities. A general wear factor is introduced to adapt the model better. Finally, the third model implements different wear factors for selected steel grades and additionally for maintenance actions. As shown in Chapter 4.5, each model has its strength.
The conclusion of this work can be summarized as follows:

- Model One shows the best overall prediction abilities as long as the conditions don't change. This means that as soon as significant changes in brick durability or maintenance material durability occur, the model will not be able to provide satisfactory predictions.
- Model Three has the best abilities to adapt to changes. Since the dataset contains a lot of faulty laser measurement data, we have not been able to show the strength of the model.
- Model Two is a trade off between the other two models. It can adapt slightly but also relies on the calculations from least squares.
- Currently, Model One provides the predictions with the smallest error and standard deviation.

5.2 Future Work

Important tasks for future work to improve the prediction of the remaining useful life of an electric arc furnace include:

- The main focus should lie on improving the quality of the laser measurements. Especially the positioning of the laser is a subject which should be thought of.
- More frequent leaser measurements improve the ability to determine how refractory wear behaves.
- Include other production parameters.
- Include data of what refractory materials have been applied since different refractory materials have different wear properties.
- Investigate possibility of sensor fusion with an optical image sensor to determine remaining slag on the refractory bricks.
- Refine the models with expert knowledge and knowledge obtained from the above points.
- Currently, each heat is considered to have the same timespan. In reality each heat duration is different. Consider the time as additional feature in the model. If the furnace cools down and is then heated again, the refractory material might behave differently.
- Reconsider the definition of the Hot Spot areas.

Bibliography

[1] American Iron and Steel Institute, "How steel is made," 2016. [Online]. Available: http://www.steel.org/making-steel/how-its-made.aspx

[2] Y. N. Toulouevski and I. Y. Zinurov, *Innovation in Electric Arc Furnaces, Scientific Basis for Selection.* Berlin, Heidelberg: Springer Berlin Heidelberg, 2013. [Online]. Available: http://www.springer.com/us/book/9783642362729

[3] G. Lammer, "Autonome Pflegeprogrammoptimierung (APO, stands for intelligent maintenance optimization) - Outline," May 2011.

[4] M. S. Grewal and A. P. Andrews, "General Information," in *Kalman Filtering.* John Wiley & Sons, Inc., 2008, pp. 1—-29. [Online]. Available: http://dx.doi.org/10.1002/9780470377819.ch1

[5] R. E. Kalman, "A New Approach to Linear Filtering and Prediction Problems," *Journal of Basic Engineering*, vol. 82, no. 1, p. 35, 1960. [Online]. Available: http://dx.doi.org/10.1115/1.3662552

[6] M. S. Grewal and A. P. Andrews, "Applications of Kalman filtering in aerospace 1960 to the present," *IEEE Control Systems Magazine*, vol. 30, no. 3, pp. 69–78, 2010. [Online]. Available: http://ieeecss.org/CSM/library/2010/june10/11-HistoricalPerspectives.pdf

[7] M. S. Grewal, *Kalman Filtering.* Berlin, Heidelberg: Springer Berlin Heidelberg, 2011, pp. 705–708. [Online]. Available: http://dx.doi.org/10.1007/978-3-642-04898-2_321

[8] G. Welch and G. Bishop, "An Introduction to the Kalman Filter," *Siggraph 2001*, no. 1, p. 81, 2001. [Online]. Available: https://www.cs.unc.edu/~welch/media/pdf/kalman_intro.pdf

[9] L. Frank, X. Lihua, and P. Dan, *Optimal and Robust Estimation: With an Introduction to Stochastic Control Theory*, 2nd ed. CRC Press, 2007. [Online]. Available: https://www.crcpress.com/Optimal-and-Robust-Estimation-With-an-Introduction-to-Stochastic-Control/Lewis-Xie-Popa/p/book/9780849390081

[10] S. Haykin, "Kalman Filters," in *Kalman Filtering and Neural Networks*, 2002, pp. 1—-21. [Online]. Available: http://dx.doi.org/10.1002/0471221546.ch1

[11] H. L. Van Trees, *Detection, Estimation, and Modulation Theory, Part I.* John Wiley & Sons, Inc., 2001, vol. 0. [Online]. Available: http://doi.wiley.com/10.1002/0471221082

[12] RHI AG, "Electronic Arc Furnace," p. 25, 2016.

[13] M. Forrer, "Prediction of refractory wear with Machine Learning methods," Master's thesis, 2012.

[14] Python Software Foundation, "Python Programming Language – Official Website," 2011. [Online]. Available: http://www.python.org/

[15] "Scientific Computing Tools for Python," 2016. [Online]. Available: https://www.scipy.org

[16] J. D. Hunter, "Matplotlib: A 2D graphics environment," *Computing in Science and Engineering*, vol. 9, no. 3, pp. 99–104, 2007. [Online]. Available: http://matplotlib.org/